AWARD NUMBER: W81XWH-14-1-0576

TITLE: Understanding and Targeting Tumor Microenvironment in Prostate Cancer to Inhibit Tumor Progression and Castration Resistance

PRINCIPAL INVESTIGATOR: Lu, Xin

CONTRACTING ORGANIZATION: MD Anderson Cancer Center
Houston, TX 77030

REPORT DATE: October 2016

TYPE OF REPORT: Annual report

PREPARED FOR: U.S. Army Medical Research and Materiel Command
Fort Detrick, Maryland 21702-5012

REPORT DOCUMENTATION PAGE

Form Approved
OMB No. 0704-0188

1. REPORT DATE	2. REPORT TYPE	3. DATES COVERED
October 2016	Annual report	30Sep2015 - 29Sep2016

4. TITLE AND SUBTITLE
Understanding and Targeting Tumor Microenvironment in Prostate Cancer to Inhibit Tumor Progression and Castration Resistance

5a. CONTRACT NUMBER

5b. GRANT NUMBER
W81XWH-14-1-0576

5c. PROGRAM ELEMENT NUMBER

6. AUTHOR(S)

Xin Lu

E-Mail: xlu3@mdanderson.org; xlu@nd.edu

5d. PROJECT NUMBER

5e. TASK NUMBER

5f. WORK UNIT NUMBER

7. PERFORMING ORGANIZATION NAME(S) AND ADDRESS(ES)

MD Anderson Cancer Center

3SCR5.4410, 1881 East Road
Houston, TX, 7054

8. PERFORMING ORGANIZATION REPORT NUMBER

9. SPONSORING / MONITORING AGENCY NAME(S) AND ADDRESS(ES)
The University of Texas MD Anderson Cancer Center
U.S. Army Medical Research and Materiel Command
Fort Detrick, Maryland 21702-5012

10. SPONSOR/MONITOR'S ACRONYM(S)

11. SPONSOR/MONITOR'S REPORT NUMBER(S)

12. DISTRIBUTION / AVAILABILITY STATEMENT

Approved for Public Release; Distribution Unlimited

13. SUPPLEMENTARY NOTES

14. ABSTRACT

The signaling mechanisms between prostate cancer cells and infiltrating immune cells may illuminate novel therapeutic approaches. In Year 2, utilizing a prostate adenocarcinoma model driven by loss of Pten and Smad4, I further validated that polymorphonuclear myeloid-derived suppressor cells (MDSCs) are the major infiltrating immune cell type and depletion of MDSCs blocks progression. Employing a novel dual reporter prostate cancer model, epithelial and stromal transcriptomic profiling identified Cxcl5 as a cancer-secreted chemokine to attract Cxcr2-expressing MDSCs and, correspondingly, pharmacological inhibition of Cxcr2 impeded tumor progression. Integrated analyses identified hyperactivated Hippo-YAP signaling in driving Cxcl5 upregulation in cancer cells through YAP-TEAD complex and promoting MDSCs recruitment. Clinico-pathological studies reveal upregulation and activation of YAP1 in a subset of human prostate tumors, and the YAP1 signature is enriched in primary prostate tumor samples with stronger expression of MDSC relevant genes. Together, YAP-driven MDSC recruitment via heterotypic Cxcl5-Cxcr2 signaling reveals effective therapeutic strategy for advanced prostate cancer.

15. SUBJECT TERMS
Prostate cancer, metastatic castration-resistant prostate cancer (mCRPC), androgen deprivation therapy (ADT) , immune checkpoint blockade (ICB), myeloid-derived suppressor cell (MDSC), Pten, Smad4, p53, YAP, CXCR2, CTLA4, PD1, chimeric mouse modeling, combination therapy

16. SECURITY CLASSIFICATION OF:			17. LIMITATION OF ABSTRACT	18. NUMBER OF PAGES	19a. NAME OF RESPONSIBLE PERSON
a. REPORT	b. ABSTRACT	c. THIS PAGE			USAMRMC
Unclassified	Unclassified	Unclassified	Unclassified	30	19b. TELEPHONE NUMBER *(include area code)*

Standard Form 298 (Rev. 8-98)
Prescribed by ANSI Std. Z39.18

Table of Contents

Page

1. INTRODUCTION

Prostate cancer (PCa) is the most common noncutaneous malignancy in men in the United States. Similar to many other solid tumor types, PCa is characterized by a rich tumor-stroma interaction network that forms the tumor microenvironment (TME)[1-3]. Among the infiltrating immune cells, myeloid-derived suppressor cells (MDSCs) represent a phenotypically heterogeneous population of immature myeloid cells that play a tumor-promoting role by maintaining a state of immunological anergy and tolerance[4]. MDSCs have been identified recently as a TME constituent in an indolent prostate cancer mouse model with conditional *Pten* deletion[5] and demonstrated to antagonize senescence during early tumorigenesis[6]. However, the molecular mechanisms underlying the recruitment of MDSCs are not well understood and the extent to which MDSCs facilitate PCa progression has not been determined, which the reported research was aimed to explore.

In Year 1, I reported that by using the *Pten*$^{pc-/-}$*Smad4*$^{pc-/-}$ metastatic PCa mouse model[7], I identified a stage-dependent increase of infiltrating and circulating granulocytic MDSCs. These MDSCs display potent immunosuppressive activity against T cell proliferation. Consistently, genes involved in ROS production, the major mechanism by which granulocytic MDSCs suppress T cells, were found highly upregulated in *Pten*$^{pc-/-}$ *Smad4*$^{pc-/-}$ tumors compared with the indolent *Pten*$^{pc-/-}$ tumors. Importantly, immuno-depletion of MDSCs with either Gr-1 antibody or a MDSC-specific peptide-Fc fusion protein[8] dramatically impeded tumor progression in *Pten*$^{pc-/-}$*Smad4*$^{pc-/-}$ mice. Preliminary results by transcriptomic profiling of cancer and non-cancer cells in the model also suggested that Cxcl5-Cxcr2 signaling may be responsible for mediating the recruitment of MDSCs to the tumor parenchyma. Therefore, my Year 1 report supported the view that targeting MDSC recruitment or activation might represent a valid therapeutic opportunity in treating advanced prostate cancer, and this effect may be most effective when combined with a modality of immunotherapy such as immune checkpoint blockade (ICB). These objectives have been explored in depth in Year 2 with results reported below.

A significant fraction of advanced PCa patients treated with androgen deprivation therapy (ADT) experience relapse with relentless progression to lethal metastatic castration-resistant prostate cancer (mCRPC)[9]. ICB has elicited durable therapeutic responses across a number of cancer types, highlighting the importance of immune evasion in tumor progression and maintenance. mCRPC exhibits increased mutational load relative to localized PCa[10], which may predict immunogenicity; an autologous cellular immunotherapy, Sipuleucel-T, has produced increase in overall survival[11]. However, the impact of ICB therapy on mCRPC has been disappointing. Specifically, anti-CTLA4 failed to significantly improve overall survival for patients with mCRPC in a Phase III trial[12], and anti-PD1 generated minimal objective responses in a Phase I trial[13]. This failure of ICB monotherapy may signal the need to combine mechanistically-distinct ICB agents and/or override additional immunosuppression mechanisms in the TME. In particular, MDSCs are known to play important roles in tumor immune evasion[14]. Correspondingly, the frequency of circulating MDSCs prior to treatment with anti-CTLA4 correlates inversely with efficacy in melanoma patients[15]. Similarly, low MDSC number is associated with improved responses to other immunotherapies such as adoptive T cell transfer[16] and tumor antigen vaccination[17]. With respect to PCa, it is notable that circulating MDSC abundance correlates with PSA levels and metastasis in patients[18-20], and that mouse models of PCa show that MDSCs ($CD11b^+$ $Gr1^+$) promote tumor initiation[6]. These observations prompted me to hypothesize that robust immunotherapy responses in mCRPC may be elicited by the combined actions of ICB agents together with targeted agents that neutralize MDSCs yet preserve T cell function. Indeed, targeting MDSCs as a cooperative approach for immunotherapy is clinically relevant, as increasing evidence indicates MDSCs represent a *bona fide* immunosuppressive cell population in patients with various solid tumors [21,22]. Immunosuppressive mechanisms by MDSCs in mice have been validated in humans, which include L-arginine depletion, NO and ROS production, TGFβ secretion, blocking T_{eff} cells and inducing T_{reg} cells, among others [21]. Future studies are warranted to evaluate if combining MDSC depletion with immune checkpoint inhibitors such as anti-CTLA4, anti-PD1 and anti-PD-L1 antibodies may elicit synergistic efficacy in the preclinical models of PCa and eventually benefit patients with prostate cancer.

2. KEYWORDS

Prostate cancer, metastatic castration-resistant prostate cancer (mCRPC), androgen deprivation therapy (ADT) , immune checkpoint blockade (ICB), myeloid-derived suppressor cell (MDSC), Pten, Smad4, p53, YAP, CXCR2, CTLA4, PD1, chimeric mouse modeling, combination therapy

3. ACCOMPLISHMENTS

- **What were the major goals of the project?**

The overall goal of the 3-year project was to provide a phenotypic and molecular understanding of MDSCs during the prostate cancer progression in the *Pten*$^{pc-/-}$*Smad4*$^{pc-/-}$ spontaneous metastatic PCa mouse model, and develop biomarkers and/or targetable molecules for MDSCs with functional and clinical validation for bench-to-bedside translation of the research. The translational value of the research is most useful if MDSC targeting can be utilized to convert the response of lethal mCRPC to immunotherapy from resistance to sensitivity. For Year 2, the specific goals included:

1) Build interactome network within the prostate cancer TME and enlist the most promising chemokine axis molecules as MDSC recruitment mechanism for *in vitro* and *in vivo* validation.
2) Identify the regulatory mechanism for activation of the MDSC-promoting chemokine pathways.
3) Provide clinical validation for the MDSC targets, thus illuminate a potential clinical path for the translation.

- **What was accomplished under these goals?**

Previously, I had incorporated *mTmG* dual fluorescence reporter allele into the *Pten*$^{pc-/-}$*Smad4*$^{pc-/-}$ model where signaling events between tumor cells and stroma can be precisely delineated. The *mTmG* allele[23] allows Cre-dependent GFP expression in prostate epithelial cells and ubiquitous tdTomato expression in all other non-Cre expressing cells (**Figure 1A**). Transcriptomic analyses of FACS-sorted GFP$^+$ tumor cells and Tomato$^+$ stromal cells showed distinct expression patterns by hierarchical clustering (Figure 1A). As proposed (**SOW Task 3**), I collaborated with Dr. Prahlad Ram and applied NetWalker, a network based genomic data analysis tool [24,25], to the transcriptomic datasets. We derived a network of connections between cancer and non-cancer cells in the TME with many of the nodes connected by chemokines and their receptors (**Figure 1B**). Through integrated analysis of the connectome result as well as the comparison of the transcriptomes of *Pten*$^{pc-/-}$*Smad4*$^{pc-/-}$ vs *Pten*$^{pc-/-}$ tumors, I identified upregulation of Cxcl5 expression in *Pten*$^{pc-/-}$*Smad4*$^{pc-/-}$ prostate neoplastic tumor cells, whereas Cxcr2, the cognate receptor for Cxcl5, is upregulated in MDSCs (see Results in Year 1 Annual Report).

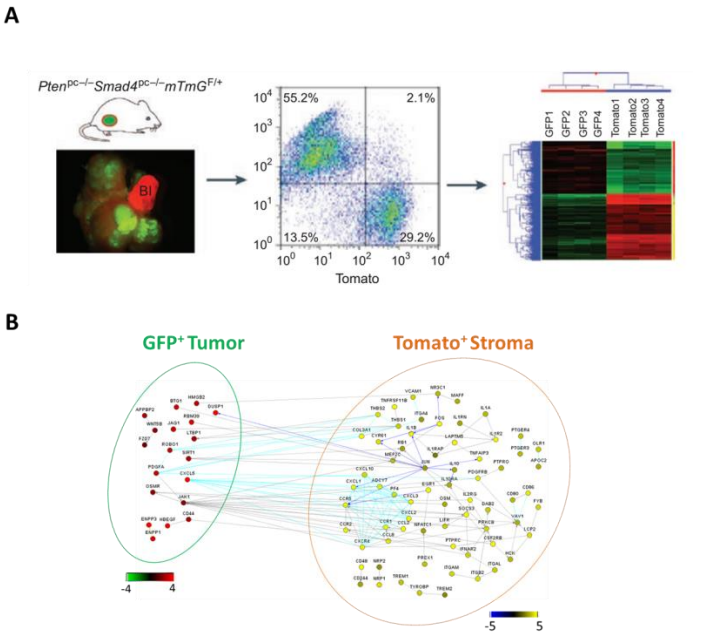

Figure 1. Transcriptomic Profiling of TME Cells in the PCa Model and Building of Connectome Using NetWalker. (A) *Pten*$^{pc-/-}$*Smad4*$^{pc-/-}$*mTmG*$^+$ model allows for FACS isolation of GFP$^+$ tumor cells and Tomato$^+$ stromal cells from the prostate adenocarcinoma, and microarray analysis to identify differentially expressed genes. **(B)** Interactome between tumor cells and stromal cells using the microarray data and constructed by NetWalker. Only secreted and membrane-associated signaling factors are shown.

To validate the Cxcl5-Cxcr2 axis in the recruitment of MDSCs to the TME of *Pten*$^{pc-/-}$*Smad4*$^{pc-/-}$ tumors, I collaborated with my colleague postdoctoral fellow, Dr. Guocan Wang, and assessed the impact of pharmacological inhibition of Cxcl5 and Cxcr2 on MDSCs using the transwell migration assay[26]. First, anti-Cxcl5 neutralizing antibody pretreatment of conditioned medium (CM) derived from *Pten*$^{pc-/-}$*Smad4*$^{pc-/-}$ prostate cancer cell line resulted in decreased migration of MDSCs (**Figure 2A**); Second, Cxcr2 inhibitor SB255002 or anti-Cxcr2 neutralizing antibody pretreatment also impeded migration of MDSCs (**Figure 2A**); Third, *in vivo* blockade of the Cxcl5-Cxcr2 axis using SB255002 in 14-week *Pten*$^{pc-/-}$*Smad4*$^{pc-/-}$ mice over a 14-day daily dosing schedule led to a dramatic

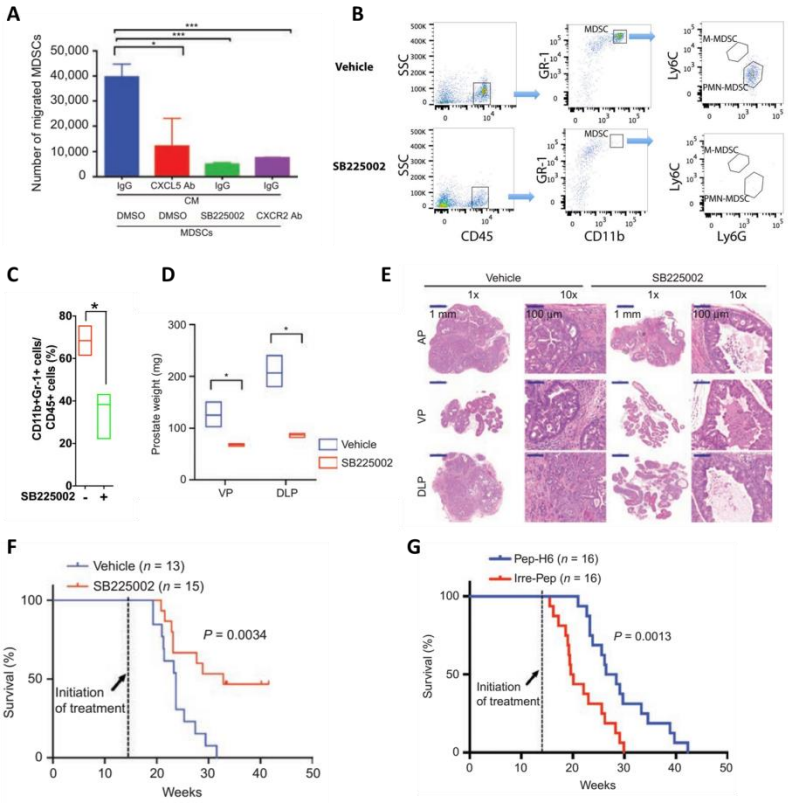

Figure 2. Cxcl5-Cxcr2 Axis Plays an Indispensable Role in Recruitment of MDSCs and Promotion of Tumor Progression. (A) Blocking the Cxcl5-Cxcr2 axis by Cxcl5 neutralizing antibody, Cxcr2 inhibitor SB225002 or Cxcr2 neutralizing antibody significantly decreased migration of MDSCs towards conditioned medium from *Pten*$^{pc-/-}$*Smad4*$^{pc-/-}$ tumors cells, evaluated with an *in vitro* transwell migration assay in triplicate. **(B-C)** SB225002 decreased MDSCs infiltration in the *Pten*$^{pc-/-}$*Smad4*$^{pc-/-}$ tumors as shown by flow cytometry analysis (n=4). **(D-E)** Cxcr2 inhibitor SB225002 treatment of *Pten*$^{pc-/-}$*Smad4*$^{pc-/-}$ mice for 14 days (n=4) resulted in significantly reduced tumor weight of VP and DLP, and significantly delayed progression for AP prostate cancer shown by H&E staining. **(F)** Cxcr2 inhibitor SB225002 treatment of *Pten*$^{pc-/-}$*Smad4*$^{pc-/-}$ mice significantly prolonged their overall survival. **(G)** Kaplan-Meier survival curve showing the significant delay of mortality caused by Pep-H6 peptibody treatment of *Pten*$^{pc-/-}$*Smad4*$^{pc-/-}$ mice.

reduction in infiltration of MDSCs in the prostate tumors (**Figure 2B-C**). Notably, similar to mice treated with anti-Gr-1 neutralizing antibody, these SB225002-treated *Pten*$^{pc-/-}$*Smad4*$^{pc-/-}$ mice also showed significant reduction in tumor burden as compared to the vehicle-treated controls (**Figure 2D**). Strikingly, all SB225002-treated tumors presented with PIN pathology while control group uniformly possessed advanced adenocarcinoma (**Figure 2E**). Furthermore, SB225002 treatment significantly prolonged the overall survival of the *Pten*$^{pc-/-}$*Smad4*$^{pc-/-}$ mice as compared to the vehicle control (**Figure 2F**). Importantly, in a different approach to depleting MDSCs, Pep-H6 peptibody treatment also provided significant survival benefit for tumor-bearing mice (**Figure 2G**). Thus through *both in vitro* and *in vivo* validations, we identified a key tumor-to-MDSC signaling axis and concluded that the Cxcl5-Cxcr2 axis plays an essential role in the recruitment of MDSCs to the *Pten*$^{pc-/-}$*Smad4*$^{pc-/-}$ prostate TME and that inhibition of this axis profoundly impairs tumor progression (**SOW Task 4.1, 4.2**).

Having identified cancer cell-derived Cxcl5 as a key signaling molecule governing recruitment of MDSCs into the TME, we sought to define the molecular mechanisms underlying the strong induction of Cxcl5 expression in the *Pten*$^{pc-/-}$*Smad4*$^{pc-/-}$ cancer cells. As Cxcl5 expression is not significantly upregulated in the *Pten*$^{pc-/-}$ tumors, we performed unbiased Gene Set Enrichment Analysis (GSEA) to identify pathways that were activated in the *Pten*$^{pc-/-}$*Smad4*$^{pc-/-}$ tumors as compared to *Pten*$^{pc-/-}$ tumors, aiming to identify potential regulators for Cxcl5 in *Pten*$^{pc-/-}$*Smad4*$^{pc-/-}$ tumors. The YAP oncogenic signature emerged as the second most hyperactivated pathway (**Figure 3A**). While it is known that the Hippo-YAP pathway plays an important role in development and cancer in organs such as liver, skin, intestine, pancreas [27-29], the role for Hippo-YAP pathway in prostate cancer biology is just emerging. Specifically, Hippo pathway components LATS1/2 have been implicated in anoikis and metastasis in prostate cancer [30] and ERG-induced Yap1 activation can promote age-related prostate tumor development [31]. However, beyond the cancer cell specific functions, the Hippo-Yap1 pathway has not been linked to signaling communication between cancer cells and immune cells in the TME. Consistent with the *in silico* analysis, IHC analysis documented a dramatic increase in the nuclear localization of Yap1 in *Pten*$^{pc-/-}$*Smad4*$^{pc-/-}$ cancer cells as compared to *Pten*$^{pc-/-}$ cancer cells (**Figure 3B**). As Yap1, a transcriptional coactivator and the downstream mediator of Hippo signaling, is regulated posttranscriptionally by either kinase-mediated degradation or cytoplasmic sequestration [27], our findings of increased nuclear localization of Yap1 is consistent with the hypothesis that Hippo-YAP pathway is activated in the *Pten*$^{pc-/-}$*Smad4*$^{pc-/-}$ tumors. In addition, unbiased oPOSSUM analysis [32] indicated that TEAD1, a member of the TEAD transcription factor family that is required for Yap1 function, ranked second among the top ten transcription factors with over-represented binding sites in

the 70 cancer-specific genes that were upregulated in the *Pten*$^{pc-/-}$*Smad4*$^{pc-/-}$ tumors as compared to the *Pten*$^{pc-/-}$ tumors (≥1.5 fold, Z-Score=13.362), an observation reinforcing the relevance of the Hippo-YAP pathway. Furthermore, we identified 6 YAP/TEAD binding motifs in the promoter of Cxcl5 gene (data not shown), suggesting Yap1 could be directly involved in the recruitment of MDSCs through regulating Cxcl5 expression. This hypothesis was supported by chromatin immunoprecipitation (ChIP) assay showing that Yap1 binds to Cxcl5 promoter (**Figure 3C**), and that shRNA-mediated knockdown of Yap1 in *Pten*$^{pc-/-}$*Smad4*$^{pc-/-}$ cancer cells drastically reduced the expression of Cxcl5 mRNA (**Figure 3D**). In addition, overexpression of a constitutively active Yap1 S127A mutant dramatically increased Cxcl5 mRNA expression in *Pten*$^{pc-/-}$*Smad4*$^{pc-/-}$ cell line (**Figure 3E**), whereas overexpression of TEAD binding defective Yap1 mutant S127A/S94A compromised its ability to activate Cxcl5 transcription (**Figure 3F**). To examine the effect of Yap1-dependent cytokine signaling in the regulation of MDSCs recruitment, we first prepared conditioned medium (CM) from *Pten*$^{pc-/-}$*Smad4*$^{pc-/-}$ cell line either infected with shRNA against Yap1 or pre-treated with Verteporfin (VP) [27], a small molecular inhibitor that disrupts Yap1-TEAD interaction. We then tested the effect of various CM on the migration of MDSCs *in vitro.* As shown in **Figure 3G-H**, we observed significantly decreased MDSCs migration *in vitro* when CM were from cells with either Yap1 knockdown or VP treatment.

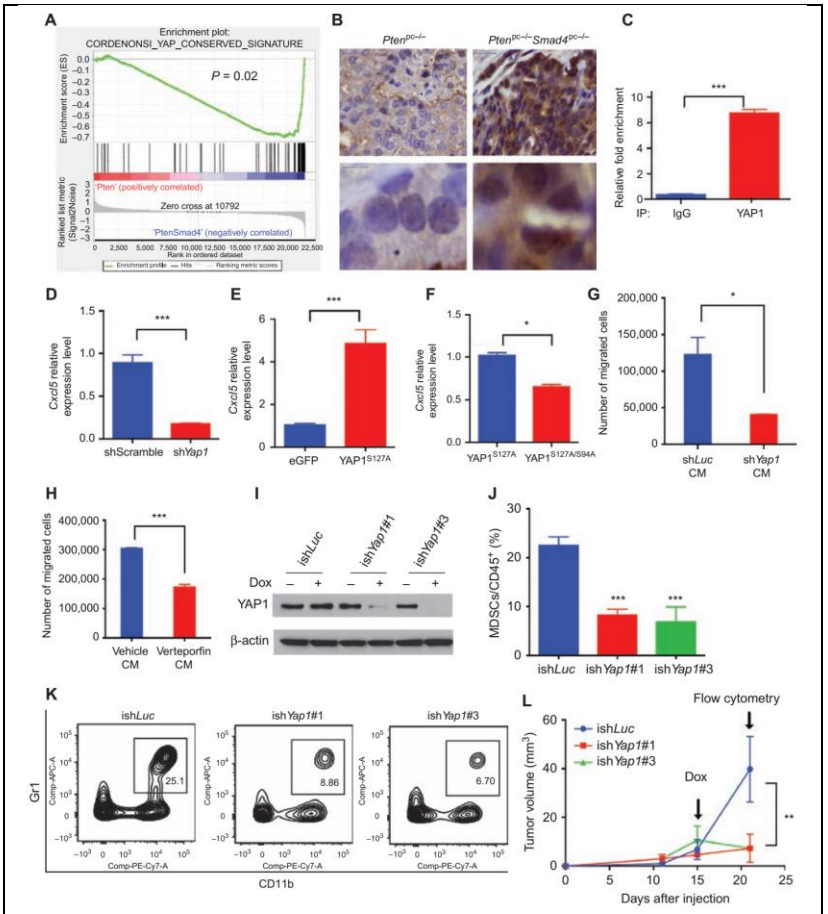

Figure 3. Hyperactivation of Yap1 in *Pten*$^{pc-/-}$*Smad4*$^{pc-/-}$ Tumors Upregulates *Cxcl5*. (A) GSEA analysis identified Yap1 oncogenic signature as the top activated pathways in the *Pten*$^{pc-/-}$*Smad4*$^{pc-/-}$ tumors compared to *Pten*$^{pc-/-}$ tumors (n=5). **(B)** A significant increase in nuclear staining of Yap1 in the *Pten*$^{pc-/-}$*Smad4*$^{pc-/-}$ tumors compared to *Pten*$^{pc-/-}$ tumors (n=3). **(C)** Chromatin immunoprecipitation shows that Yap1 can directly bind to *Cxcl5* promoter using quantitative PCR in triplicates. **(D)** shRNA knockdown of Yap1 in *Pten*$^{pc-/-}$*Smad4*$^{pc-/-}$ tumor cells resulted in a dramatic reduction in Cxcl5 mRNA expression using quantitative PCR in triplicates. **(E)** Overexpression of a constitutively active YAP1 S127A mutant resulted in upregulation of *Cxcl5* mRNA using quantitative PCR in triplicates. **(F)** TEAD-binding defective S127A/S94A Yap1 mutant significantly decreased *Cxcl5* mRNA expression as compared to the Yap1 S127A mutant using quantitative PCR in triplicates. **(G-H)** Conditioned medium prepared from *Pten*$^{pc-/-}$*Smad4*$^{pc-/-}$cells infected with Yap1 shRNA (G) or treated with Verteporfin (H), a small molecule that disrupts Yap1-TEAD interaction, induced less MDSCs migration *in vitro* as compared to the control conditioned medium. Transwell migration was done in triplicate for each condition. **(I)** Western blot analysis showed that two independent inducible shRNAs for Yap1 efficiently knockdown Yap1 expression in the *Pten*$^{pc-/-}$*Smad4*$^{pc-/-}$cells. **(J-L)** Inducible Yap1 knockdown strongly suppressed the intratumoral MDSC infiltration (J-K) and tumor growth (L) of the C57BL/6-syngeneic cell line isolated from prostate tumor of *Pten*$^{pc-/-}$*Smad4*$^{pc-/-}$*Trp53*$^{pc-/-}$ mice (n=5). In **C, D, E** and **F, G, H, L** ***P<0.01, ***P<0.001.*

Finally, to test if targeting Yap1 *in vivo* can impair the infiltration of MDSCs and inhibit tumor growth, we used our recently isolated syngeneic murine prostate cancer line PPS, which is derived from the backcrossed *Pten*$^{pc-/-}$*Smad4*$^{pc-/-}$*Tp53*$^{pc-/-}$ model[33] and can form subcutaneous or orthotopic tumors robustly in C57BL/6 hosts. Doxycycline-dependent shRNA knockdown of Yap1 (two independent shRNA designs #1 and #3) were established in PPS (**Figure 3I**), and injected subcutaneously in C57BL/6 mice. Yap1 knockdown induced by switching to doxycycline-containing drinking water resulted in a reduction of MDSCs in the intratumoral CD45^{+} population (**Figure 3 J-K)** and impaired tumor progression (**Figure 3L**). While the observation supports the hypothesis that targeting YAP1-dependent MDSC infiltration impairs tumor growth, we acknowledge that the tumor growth impediment by Yap1 silencing is likely due to a combined effect of both cell non-autonomous and autonomous mechanisms.

Together, these findings reveal a novel function for Yap1 in the recruitment of MDSCs through direct upregulation of Cxcl5 transcription in prostate tumor cells. These results build stronger rationale and methodology on MDSC targeting and indicate the achievement of the milestone for the **SOW Major Task 4**.

Clinicopathology validation of druggable molecules mediating tumor-MDSC interaction in PCa is the **5th (and the last) Major Task** for the SOW, and I had made significant progress in this direction as well in Year 2. To determine whether YAP1 is overexpressed and activated in human prostate cancer, we performed immunohistochemical staining of human prostate cancer tissue microarray (TMA, purchased from US Biomax Tissue Microarray) for YAP1. Interestingly, YAP1 is expressed in basal cells, but not in the luminal cells of the normal human prostate (**Figure 4A**). In addition, we observed YAP1 is overexpressed in a subset of human prostate cancers (**Figure 4A-B**), consistent with a recent report [31]. Given the lack of validated antibodies for human MDSCs for TMA analysis, I generated a list of 39 MDSC related genes curated from literature analysis to generate evidence of a link between YAP1 activation and MDSC prominence in human prostate. Using the prostate TCGA RNA-seq data, unsupervised clustering with the 39-gene MDSC signature categorized 498 TCGA primary prostate tumors into three subtypes: MDSC-high (n=139), MDSC-medium (n=158), and MDSC-low (n=201) (**Figure 4C**), suggesting that a subset of human prostate tumors may have prominent infiltration of MDSCs. In addition, using GSEA, I found that several YAP1 signature genes are significantly overexpressed in MDSC-high samples as compared to MDSC-low samples (**Figure 4D**; p value < 0.005), reinforcing the link between MDSC-high prostate tumors and YAP1 transcriptional activities. Furthermore, CXCL6, the human homologue of murine Cxcl5, is expressed at a higher levels in the MDSC-high samples as compared to MDSC-low samples (Figure 4E, p=9.40E-29). Similar analysis was performed in a published dataset focused on tumor immunobiological differences in prostate cancer between African-American and European-American men[34]. The 39-gene MDSC signature can cluster the 69 primary prostate tumors into MDSC-high (n=40) and MDSC-low (n=29) and Yap1 signatures were prominent in the MDSC-high groups (data not shown). Together, these human prostate tumor findings, which parallel our murine observations, suggest that activated YAP1 is integral to MDSCs infiltration in both mouse and human prostate cancer, thus enhancing the translational value of the study. **The results described above, together with the results described in Year 1 Report, have been published recently (Wang*, Lu*, *Cancer Discovery*, 2016. *Equal contribution)[35] and attached as Appendix.**

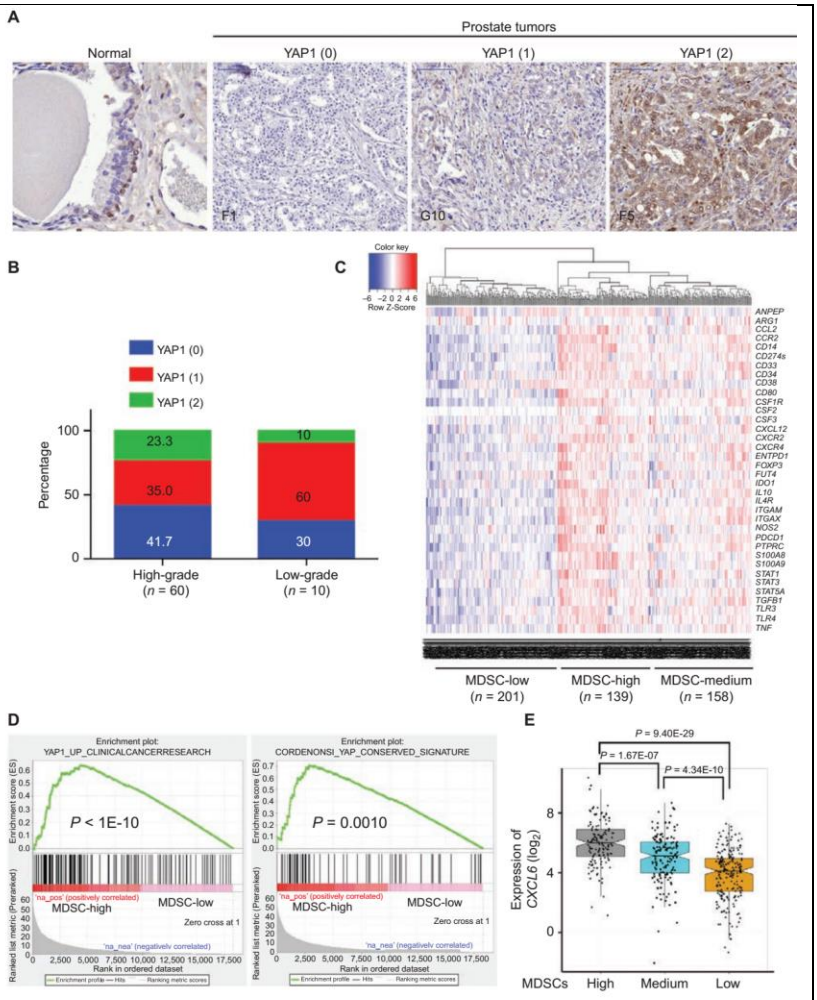

Figure 4. YAP1 is activated in human prostate cancer and correlated with MDSCs signature and CXCL6 (human homolog of mouse Cxcl5) overexpression. (A) IHC analysis of YAP1 expression in basal cells of normal prostate tissue and human prostate cancers. Numbers in parenthesis indicates YAP1 IHC scores. **(B)** YAP1 IHC score representation in low grade (n=10) and high grade (n=60) prostate cancer. **(C)** Clustering of human TCGA prostate samples into MDSC-high, MDSC-low and MDSC-medium groups using a 39-gene MDSC signature. **(D)** YAP1 signatures are identified in MDSC-high prostate TCGA samples. **(E)** CXCL6 expression is significantly higher in MDSC-high group.

In summary, through Year 1 and Year 2, I have accomplished the majority of the experiments proposed in the three Aims in the original Narrative and SOW, with the following subtasks unfinished yet: (1) Perform tumor-MDSC recombination experiment to evaluate the tumor-promoting function of MDSCs; (2) RPPA and cytokine array of MDSCs and associated tumor cells; (3) MDSC-to-tumor signaling validation with in vitro and in vivo assays. Importantly, I have published the data collected and supported by this grant, thus achieved a major delivery of the proposal. While it is clear that the unfinished experiments would be still very interesting and important to pursue in Year 3, I propose to deprioritize them and changes in the SOW for Year 3, because, as stated in the **Introduction**, my studies in MDSCs urge me and my team to evaluate if combining MDSC depletion with immune checkpoint inhibitors such as anti-CTLA4 and anti-PD1 antibodies may elicit synergistic efficacy in the preclinical models of PCa and eventually benefit patients with prostate cancer. Please refer to my request on changes of SOW for more justification and rationale on the proposed changes. Below, I would like to present some data that I generated recently through different funding mechanisms (Startup fund for Dr. DePinho and internal funding in the Institute of Advanced Cancer Science [IACS] at MD Anderson Cancer Center), in a collaboration between me and IACS at MD Anderson. While they are not directly related to the Specific Aims, they form the foundation for what I propose as changes for the SOW for Year 3. All the animal works in the data described below were approved by The University of Texas MD Anderson Cancer Center Institutional Animal Care and Use Committee (IACUC) with aforementioned separate funding mechanisms.

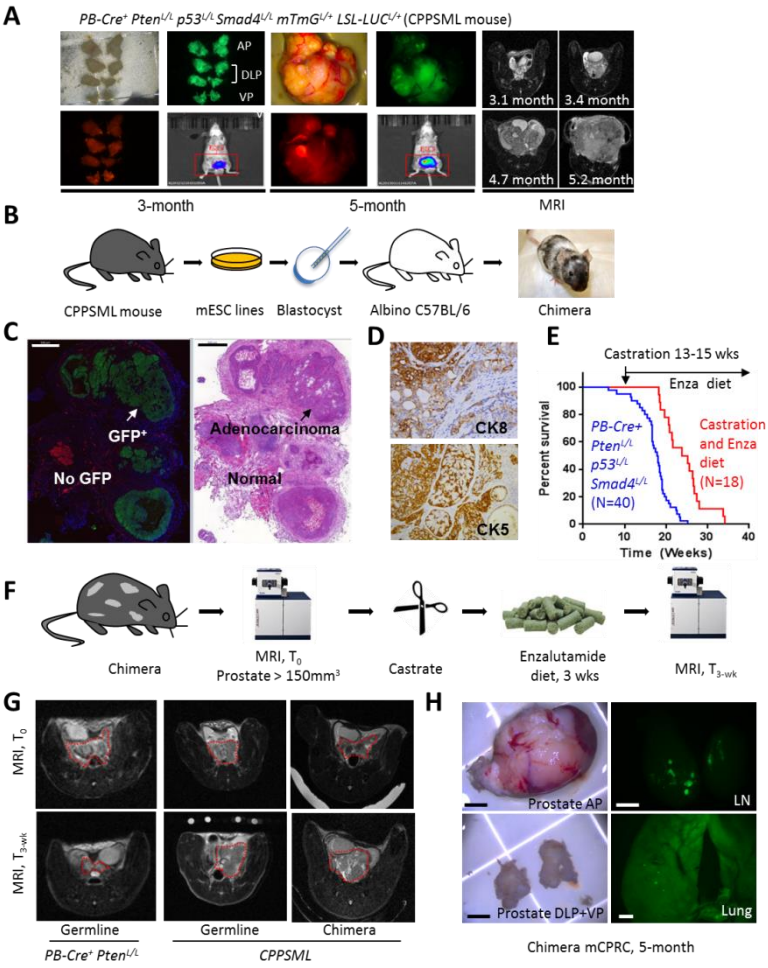

Figure 5. Establishment of the CPPSML chimera model of metastatic castration-resistant prostate cancer. (A) The spontaneous prostate tumor development in *PB-Cre*$^{+}$ *Pten*$^{L/L}$ *p53*$^{L/L}$ *Smad4*$^{L/L}$ *mTmG*$^{L/+}$ *LSL-LUC*$^{L/+}$ (CPPSML) mice with tumor detection by whole organ fluorescence imaging, bioluminescence imaging and MRI. **(B)** Generation of the CPPSML chimera model. **(C)** Fluorescence microscopy and H&E image of snap frozen prostate tumor from chimera showing that the GFP^{+} area corresponds to adenocarcinoma and the GFP^{-} area corresponds to normal host cells. Scale bar 500μm. **(D)** IHC staining showing the expansion of both CK8^{+} luminal lineage and CD5^{+} basal lineage in the prostate tumor formed in CPPSML chimera. **(E)** Significant (P<0.0001, Log-rank test) yet transient survival benefit by castration followed by diet admixed with enzalutamide (50mg/kg diet) in *PB-Cre*$^{+}$ *Pten*$^{L/L}$ *p53*$^{L/L}$ *Smad4*$^{L/L}$ mice (n=40 and 18, respectively). **(F)** Procedure for testing chimera response to castration and enzalutamide diet. **(G)** Comparison of MRI images at T_0 and $T_{3\text{-wk}}$ showing the regression of *PB-Cre*$^{+}$ *Pten*$^{L/L}$ prostate tumors after castration/Enza treatment yet the resistance of CPPSML mice (either from germline breeding or chimera) to such treatment (n=5). **(H)** Representative CPPSML chimera with primary CRPC, lymph node metastasis, and micrometastasis in lung. Scale bar: prostate 5mm; lymph node and lung, 1mm. In (a) and (h), AP, DLP and VP denote anterior, dorsolateral and ventral prostate lobes, respectively.

Theoretically, mouse models of PCa, such as the *Pten*$^{pc-/-}$*Smad4*$^{pc-/-}$ model (also denoted as *PB-Cre*$^{+}$ *Pten*$^{L/L}$ *Smad4*$^{L/L}$) and the *Pten*$^{pc-/-}$ *p53*$^{pc-/-}$*Smad4*$^{pc-/-}$ model (also denoted as *PB-Cre*$^{+}$ *Pten*$^{L/L}$ *p53*$^{L/L}$ *Smad4*$^{L/L}$), have been generated and can be used for testing the hypothesis on combined targeted and immune therapies, thanks to their autochthonous tumor evolution in an intact immune system. However, for preclinical therapeutic testing, traditional germline genetically engineered mouse models (GEMMs) with multiple alleles have limited capacity to generate the number of mice needed to conduct a multi-arm drug testing protocol. This issue is particularly pressing for PCa models based on *PB-Cre*, the most widely used Cre driver for conditional deletion of key tumor suppressors in the mouse

prostate epithelium[36]. In these models, optimal intercrosses produce 12.5% PCa-prone males in a litter. I sought to overcome this experimental shortcoming through development of a novel metastatic PCa model that employs recent technical advances in non-germline GEMMs[37,38]. The DePinho lab had previously generated a germline model of metastatic PCa engineered with the *PB-Cre*$^{+}$ *Pten*$^{L/L}$ *p53*$^{L/L}$ *Smad4*$^{L/L}$ genotype[39]. To enhance this model for TME and immunotherapy studies, I bred in the Cre-activated reporter *ROSA26-Lox-tdTomato-Lox-EGFP* (*mTmG*)[23] and *ROSA26-pCAGGs-LSL-luciferase* (developed by Dr. Tyler Jacks) followed by backcross to the C57BL/6 background. The resultant mice with genotype *PB-Cre*$^{+}$ *Pten*$^{L/L}$ *p53*$^{L/L}$ *Smad4*$^{L/L}$ *mTmG*$^{L/+}$ *LSL-LUC*$^{L/+}$ (CPPSML) exhibited age-dependent GFP^{+} LUC^{+} metastatic PCa development monitored by bioluminescence imaging as well as MRI for optimal tumor detection and volume calculation (**Figure 5A**).

To expedite the generation of PCa-bearing CPPSML mice, I worked together with the transgenic core within the IACS at MD Anderson and established *PB-Cre*$^{+}$ *Pten*$^{L/L}$ *p53*$^{L/L}$ *Smad4*$^{L/L}$ *mTmG*$^{L/+}$ *LSL-LUC*$^{L/+}$ mouse embryonic stem cell (mESC) clones (JH61 and JH58) from the CPPSML model. The mESC lines were verified to be of normal karyotype and congenic to C57BL/6 through genomic loci including the MHC H2 complex H2^{b} (data not shown). Employing blastocyst complementation, JH61 or JH58 mESCs were injected into blastocysts derived from albino C57BL/6 mice (**Figure 5B**), producing CPPSML chimeras with comparable PCa development that is largely dependent on the contribution of CPPSML mESCs in chimeric prostate organ (data not shown). In high percentage chimeras (79.1% of chimeras had >75% coat color contributed by injected mESCs, 50% of mice (4/8 necropsied) developed GFP^{+} cancer cells at 3 months of age and showed dissemination of cancer cells to draining lymph nodes and lung, which mirrored the phenotype of the germline model[33] (data not shown). At the histological level, GFP^{+} areas corresponded to CK8^{+}/CK5^{+} prostate adenocarcinoma, while GFP^{-} areas exhibited normal glandular morphology (**Figure 5C-D**). It is worth noting the significant increase in the rate of generating PCa-bearing mice from 12.5% through breeding to 53.6% through chimeric modeling.

To study combination therapy in the context of mCRPC, I first employed the *PB-Cre*$^{+}$ *Pten*$^{L/L}$ *p53*$^{L/L}$ *Smad4*$^{L/L}$ germline model and demonstrated that an androgen deprivation therapy (ADT) protocol (castration followed by enzalutamide-admixed diet) generated a significant, albeit transient, survival benefit (**Figure 5E**). At necropsy, all treated mice had large primary CRPC (N=18, data not shown). Next, CPPSML chimeras were subjected to the same ADT to induce CRPC. To ensure consistency, MRI was used to enroll chimeras with prostate tumor volumes over 150mm^{3} before 18 weeks of age – in total 86/107 (80.4%) chimeras achieved this experimental objective (**Figure 5F**). I validated emergence of CRPC in CPPSML chimeras by comparing the response of size-matched primary prostate tumors to ADT in three cohorts: the chimeras, CPPSML mice through breeding, and *PB-Cre*$^{+}$ *Pten*$^{L/L}$ mice (**Figure 5G**). All treated chimeras succumbed to primary CRPC, with mCRPC in draining lymph nodes and micrometastases in lungs (**Figure 5H**). These results indicated that the CPPSML chimeras develop mCRPC and thus are capable of serving as a speedy platform to test therapies for mCRPC, in particular, the combination of therapy that targets MDSCs with ICB agents such as anti-CTLA4 and/or anti-PD1. The CPPSML chimeric model has formed the foundation for my proposed changes in the SOW for Year 3.

References

1 Karlou, M., Tzelepi, V. & Efstathiou, E. *Nat Rev Urol* **7**, 494-509 (2010).
2 Junttila, M. R. & de Sauvage, F. J. *Nature* **501**, 346-354 (2013).
3 Hanahan, D. & Coussens, L. *Cancer Cell* **21**, 309-322 (2012).
4 Talmadge, J. E. & Gabrilovich, D. I. *Nat Rev Cancer* **13**, 739-752 (2013).
5 Garcia, A. J. *et al. Molecular and cellular biology* **34**, 2017-2028 (2014).
6 Di Mitri, D. *et al. Nature* **515**, 134-137 (2014).
7 Ding, Z. *et al. Nature* **470**, 269-273 (2011).
8 Qin, H. *et al. Nat Med* **20**, 676-681 (2014).
9 Watson, P. A., Arora, V. K. & Sawyers, C. L. *Nat Rev Cancer* **15**, 701-711 (2015).
10 Robinson, D. *et al. Cell* **161**, 1215-1228 (2015).
11 Kantoff, P. W. *et al. N Engl J Med* **363**, 411-422 (2010).
12 Kwon, E. D. *et al. The Lancet Oncology* **15**, 700-712 (2014).

13 Topalian, S. L. *N. Engl. J. Med.* **366**, 2443-2454 (2012).
14 Gabrilovich, D. I. & Nagaraj, S. *Nat Rev Immunol* **9**, 162-174 (2009).
15 Meyer, C. *et al. Cancer immunology, immunotherapy : CII* **63**, 247-257 (2014).
16 Wang, Z. *et al. Journal of immunotherapy (Hagerstown, Md. : 1997)* **37**, 43-50 (2014).
17 Kimura, T. *et al. Cancer Prev Res* **6**, 18-26 (2013).
18 Vuk-Pavlović, S. *et al. Prostate* **70**, 443-455 (2010).
19 Brusa, D. *et al. Int J Urol* **2013**, 12086 (2013).
20 Hossain, D. M. *et al. Clin Cancer Res* (2015).
21 Filipazzi, P., Huber, V. & Rivoltini, L. *Cancer Immunology, Immunotherapy* **61**, 255-263 (2012).
22 Solito, S. *et al. Ann N Y Acad Sci* **1319**, 47-65 (2014).
23 Muzumdar, M. D., Tasic, B., Miyamichi, K., Li, L. & Luo, L. *Genesis* **45**, 593-605 (2007).
24 Komurov, K., White, M. A. & Ram, P. T. *PLoS Computational Biology* **6** (2010).
25 Komurov, K., Dursun, S., Erdin, S. & Ram, P. T. *BMC Genomics* **13** (2012).
26 Yang, L. *et al. Cancer Cell* **13**, 23-35 (2008).
27 Johnson, R. & Halder, G. *Nat Rev Drug Discov* **13**, 63-79 (2014).
28 Kapoor, A. *et al. Cell* **158**, 185-197 (2014).
29 Shao, D. D. *et al. Cell* **158**, 171-184 (2014).
30 Zhao, B. *et al. Genes & development* **26**, 54-68 (2012).
31 Nguyen, L. T. *et al. Cancer Cell* **27**, 797-808 (2015).
32 Kwon, A. T., Arenillas, D. J., Worsley Hunt, R. & Wasserman, W. W. *G3* **2**, 987-1002 (2012).
33 Ding, Z. *et al. Cell* **148**, 896-907 (2012).
34 Wallace, T. A. *et al. Cancer Res* **68**, 927-936 (2008).
35 Wang, G. *et al. Cancer Discov* **6**, 80-95 (2016).
36 Shen, M. M. & Abate-Shen, C. *Genes & Development* **24**, 1967-2000 (2010).
37 Heyer, J., Kwong, L. N., Lowe, S. W. & Chin, L. *Nat Rev Cancer* **10**, 470-480 (2010).
38 Huijbers, I. J. *et al. Nat. Protocols* **10**, 1755-1785 (2015).
39 Ding, Z. *et al. Cell* **148**, 896-907 (2012).

- **What opportunities for training and professional development has the project provided?**

Professional development: With the conducted research supported by the grant, the PI Xin Lu had the opportunity for the following conferences and workshops:
1) BD Biosciences course "Multicolor Flow Cytometry - Beyond the Basics". **Certificate awarded**. Sep 16-18, 2014. San Jose, CA
2) Society For Immunotherapy of Cancer (SITC) Annual Meeting. Nov 6-9, 2014, National Harbor, MD
3) 22nd Annual Prostate Cancer Foundation (PCF) Scientific Retreat. **Poster presentation**. Oct 8-10, 2015. Washington, DC
4) American Physical Society March Meeting, **Invited speaker**. Mar 18, 2016. Baltimore, MD
5) DoD Prostate Cancer Research Program (PCRP) IMPaCT 2016 conference, **Oral presentation**. Aug 4-5, 2016. Towson, MD

- **How were the results disseminated to communities of interest?**

The results, presented in conferences and through publication, have attracted collaborations from prominent scientists and companies in the fields of prostate cancer and immunotherapy, including Dr. Padmanee Sharma, Dr. Patricia Troncoso at MD Anderson Cancer Center, Dr. Marcin Kortylewski at City of Hope, Duarte, CA, and Syntrix Biosystems which develops novel chemokine receptor inhibitors.

The research has also attracted interests from young professionals including three individuals who have participated in the study under the supervision of Xin Lu: **Sunada Khadka**, CPRIT-CURE Summer Intern at MD Anderson Cancer Center, college student at Wesleyan College, Macon, Georgia; **Ashwin Varma**, college student at Rice University, Houston, Texas; **Jeong Woo Han**, high school sophomore, Michael E. DeBakey

HSHP, Houston, Texas. All students expressed strong interest in career on biomedical research after exposed in this research project, and Sunada has started her PhD program at MD Anderson Cancer Center.

- **What do you plan to do during the next reporting period to accomplish the goals?**

I plan to advance the translational studies on MDSC targeting in prostate cancer through changes to the SOW for Year 3. In particular, I propose to unitize my newly developed CPPSML chimeric models of mCRPC and combine MDSC-targeting strategies with immune checkpoint blockade agents anti-CTLA4 and anti-PD1 to test the combination efficacy compared with individual treatments. The following goals should be achieved:
1) Select drugs that not only effectively deplete MDSCs in the TME of the model, but also have preexisting significant clinical developments so that the combination efficacy, if observed in the preclinical models, can be translated soon into early phase clinical trials.
2) Perform single and combination therapies in the mCRPC chimeric model (vehicle and isotype IgG control, anti-MDSC agent, ICB agent, combination), and evaluate the response by both primary tumors and metastases in lymph nodes and lung.
3) Explore the mechanism of combination efficacy through CyTOF-based immunophenotyping, antibody array-based signaling studies and *in vitro* functional assays, to determine if the hypothesis on enhancing immunotherapy through MDSC targeting is supported by experimental evidence.
4) Collaborate with Dr. Troncoso to perform immunophenotyping of human prostate cancer fresh samples to validate the preclinical observations.

4. IMPACT

- **What was the impact on the development of the principal discipline(s) of the project?**

While Year 1 research has built a solid foundation on the functional importance of the myeloid derived suppressor cells (MDSCs) in the progression of prostate cancer in the transgenic mouse models, Year 2 research advanced the study to show that mechanism-based targeting strategy, in particular, blocking either Cxcr2 or YAP signaling, significantly impedes the development of the cancer, in terms of both tumor size as well as histopathology. Importantly, the findings have significant clinical relevance as both the YAP signature and CXCL6 (Cxcl5 homolog in human) showed strong correlation with the MDSC signature in prostate cancer. Our results, as published in *Cancer Discovery*, have made important contribution to the fields of prostate cancer and tumor microenvironment.

- **What was the impact on other disciplines?**

The finding that MDSCs are potent immunosuppressors in the tumor microenvironment of prostate cancer has an overarching impact on the field of immunotherapy. Immunotherapy has been established as an additional pillar in the treatment of cancer, especially with recent development of immune checkpoint blockers like anti-PD1 and anti-CTLA4 antibodies. Nevertheless, the immunotherapy on prostate cancer and some other cancer types using such immune checkpoint blockade approach as monotherapy has been unsuccessful so far. My result suggests that combination targeting of both T cells and immunosuppressive cells such as MDSCs may hold the promise for synergistic efficacy to achieve better performance of cancer immunotherapy for prostate cancer and possibly other cancer types. I plan to specifically address this hypothesis in Year 3.

- **What was the impact on technology transfer?**

At the completion of Year 2 of proposed research, there is nothing to report on this aspect yet.

- **What was the impact on society beyond science and technology?**

At the completion of Year 2 of proposed research, there is nothing to report on this aspect yet.

5. CHANGES/PROBLEMS

Changes in approach and reasons for change

In Year 1, I closely followed the original SOW and performed most of the experiments proposed and obtained promisng results indicating: (1) $CD11b^+$ $Gr\text{-}1^+$ myeloid-derived suppressor cells (MDSCs) are significantly

increased in *Pten*$^{pc-/-}$*Smad4*$^{pc-/-}$ prostate tumors as compared to *Pten*$^{pc-/-}$ tumors in the mouse models; (2) MDSCs from *Pten*$^{pc-/-}$*Smad4*$^{pc-/-}$ tumors display potent immunosuppressive activities and are dominated by PMN-MDSCs. (3) Targeting MDSCs with anti-Gr-1 neutralizing antibody or MDSC-specific peptibody significantly delayed tumor progression in *Pten*$^{pc-/-}$*Smad4*$^{pc-/-}$ Mice; (4) *Pten*$^{pc-/-}$*Smad4*$^{pc-/-}$ prostate tumors enrich for MDSCs with higher Cxcr2 expression, and Cxcl5-Cxcr2 axis may be relevant to the recruitment of MDSCs. These results and conclusions were reported in Year 1 Annual Report. In Year 2, I further reported the results on the validation of the Cxcl5-Cxcr2 signaling as the key pathway for recruiting MDSCs and the identification of YAP pathway as the mechanism for controlling the upregulation of the Cxcl5-Cxcr2 paracrine signaling. Moreover, I reported the results on the clinical validation using both in silico data as well as TMA. These results were generated to fulfill the Specific Aim 2 and Aim 3 of the Project and associated tasks in the SOW.

The goal of the project was set to understanding the key immunocyte population and mechanism for creating the immunosuppressive tumor microenvironment in metastatic prostate cancer (with its most deadly form as castration resistant prostate cancer, or CRPC) and developing effective treatment for metastatic prostate cancer by therapeutic targeting of MDSCs. Year 1 results in fact have already illuminated a two-step path for achieving the translational objective of the project: **Step 1**, demonstrate that target MDSCs using reagents blocking Cxcl5-Cxcr2 signaling or YAP signaling can inhibit prostate cancer progression in the mouse models, and show clinical validation using in silico and clinical specimens; **Step 2**, combine MDSC targeting with immunotherapy to enhance the efficacy. Collaborating with my colleague, I have finished Step 1 in Year 2 and published the results in *Cancer Discovery*. Through such efforts, I have achieved major deliveries for Major Task 3/4/5 in the original SOW, although there remain unfinished subtasks as described above, including (1) Perform tumor-MDSC recombination experiment to evaluate the tumor-promoting function of MDSCs; (2) RPPA and cytokine array of MDSCs and associated tumor cells; (3) MDSC-to-tumor signaling validation with in vitro and in vivo assays.

For Step 2, an obvious choice of immunotherapy to combine with in our mouse models is immune checkpoint blockade antibodies. Immune checkpoint blockade (ICB) using anti-CTLA4 and/or anti-PD1 generates durable therapeutic responses in a meaningful subset of patients across a variety of cancer types. However, in metastatic CRPC, ICB monotherapy has shown minimal activity, motivating search for regimens that combine ICB drugs with genetically targeted therapies. Combined targeted therapy with immunotherapy represents a new research area of preclinical and clinical cancer treatment that has generated tremendous excitement and progress in the last couple years. Our results showing the essential role of MDSCs in prostate cancer may potentially hit a missing piece in effective immunotherapy using ICB agents. At the same time as I started to think about combination therapy, a major technical breakthrough occurred in my collaboration with the Institute of Advanced Cancer Science at MD Anderson Cancer Center: we created the first embryonic stem cell (ESC)-based chimeric model of metastatic CRPC. This model provides an efficient platform for testing combination therapy in a spontaneous tumor development setting with intact immune system. Therefore, a golden opportunity is presenting itself for me to merge my idea of targeting MDSCs with this new model to test whether combining MDSC-targeting drugs with ICB agents could generate synergistic effect in controlling or even curing mCRPC. I think this represents changes in approach in the SOW with well justified reasons, as the changes have the potential to improve our view on how to design clinical trials on ICB in treating mCRPC, which have all failed so far. **Most importantly, the proposed changes fall in the original scope of the project.**

I was invited to give an oral presentation of the preliminary data for the proposed new works at the PCRP - Innovative Minds in Prostate Cancer Today (IMPaCT) 2016 meeting, and these new directions were highly

regarded by leaders and colleagues in the field. For details of the proposed SOW changes, please refer to the SOW document, submitted also in October 2016.

6. PRODUCTS

Publications

Wang, G*., Lu, X*., Dey, P., Deng, P., Wu, C. C., Jiang, S., Fang, Z., Zhao, K., Konaparthi, R., Hua, S., *et al.* (2016). Targeting YAP-Dependent MDSC Infiltration Impairs Tumor Progression. Cancer Discov *6*, 80-95. (*Equal contribution)

7. PARTICIPANTS & OTHER COLLABORATING ORGANIZATIONS

- **What individuals have worked on the project?**

Name:	*Xin Lu*
Project Role:	*Instructor*
Researcher Identifier (e.g. ORCID ID):	
Nearest person month worked:	*8*
Contribution to Project:	*No change*
Funding Support:	*No change*

Name:	*Guocan Wang*
Project Role:	*Postdoc Fellow*
Researcher Identifier (e.g. ORCID ID):	*Not applicable*
Nearest person month worked:	*6*
Contribution to Project:	*Dr. Wang has co-performed the works on identification and validation of YAP signaling, as well as part of the clinical validation studies. Dr. Wang also contributed equally to the writing and revision of the manuscript in Cancer Discovery.*
Funding Support:	Institutional funds

- **Has there been a change in the active other support of the PD/PI(s) or senior/key personnel since the last reporting period?**

Nothing to report.

- **What other organizations were involved as partners?**

Nothing to report.

8. SPECIAL REPORTING REQUIREMENTS

Nothing to report.

9. APPENDICES:

Wang, G*., Lu, X*., Dey, P., Deng, P., Wu, C. C., Jiang, S., Fang, Z., Zhao, K., Konaparthi, R., Hua, S., *et al.* (2016). Targeting YAP-Dependent MDSC Infiltration Impairs Tumor Progression. Cancer Discov *6*, 80-95. (*Equal contribution)

Published OnlineFirst December 23, 2015; DOI: 10.1158/2159-8290.CD-15-0224

RESEARCH ARTICLE

Targeting YAP-Dependent MDSC Infiltration Impairs Tumor Progression

Guocan Wang[1,2], Xin Lu[1,2], Prasenjit Dey[1,2], Pingna Deng[1,2], Chia Chin Wu[3], Shan Jiang[2], Zhuangna Fang[2,4], Kun Zhao[2], Ramakrishna Konaparthi[2], Sujun Hua[1,2], Jianhua Zhang[3], Elsa M. Li-Ning-Tapia[5], Avnish Kapoor[2], Chang-Jiun Wu[3], Neelay Bhaskar Patel[2], Zhenglin Guo[1], Vandhana Ramamoorthy[3], Trang N. Tieu[3], Tim Heffernan[3], Di Zhao[1,2], Xiaoying Shang[1], Sunada Khadka[1], Pingping Hou[1,2], Baoli Hu[1,2], Eun-Jung Jin[1,6], Wantong Yao[2], Xiaolu Pan[2], Zhihu Ding[7], Yanxia Shi[2,4], Liren Li[2,4], Qing Chang[3], Patricia Troncoso[8], Christopher J. Logothetis[5], Mark J. McArthur[9], Lynda Chin[2], Y. Alan Wang[1,2], and Ronald A. DePinho[1]

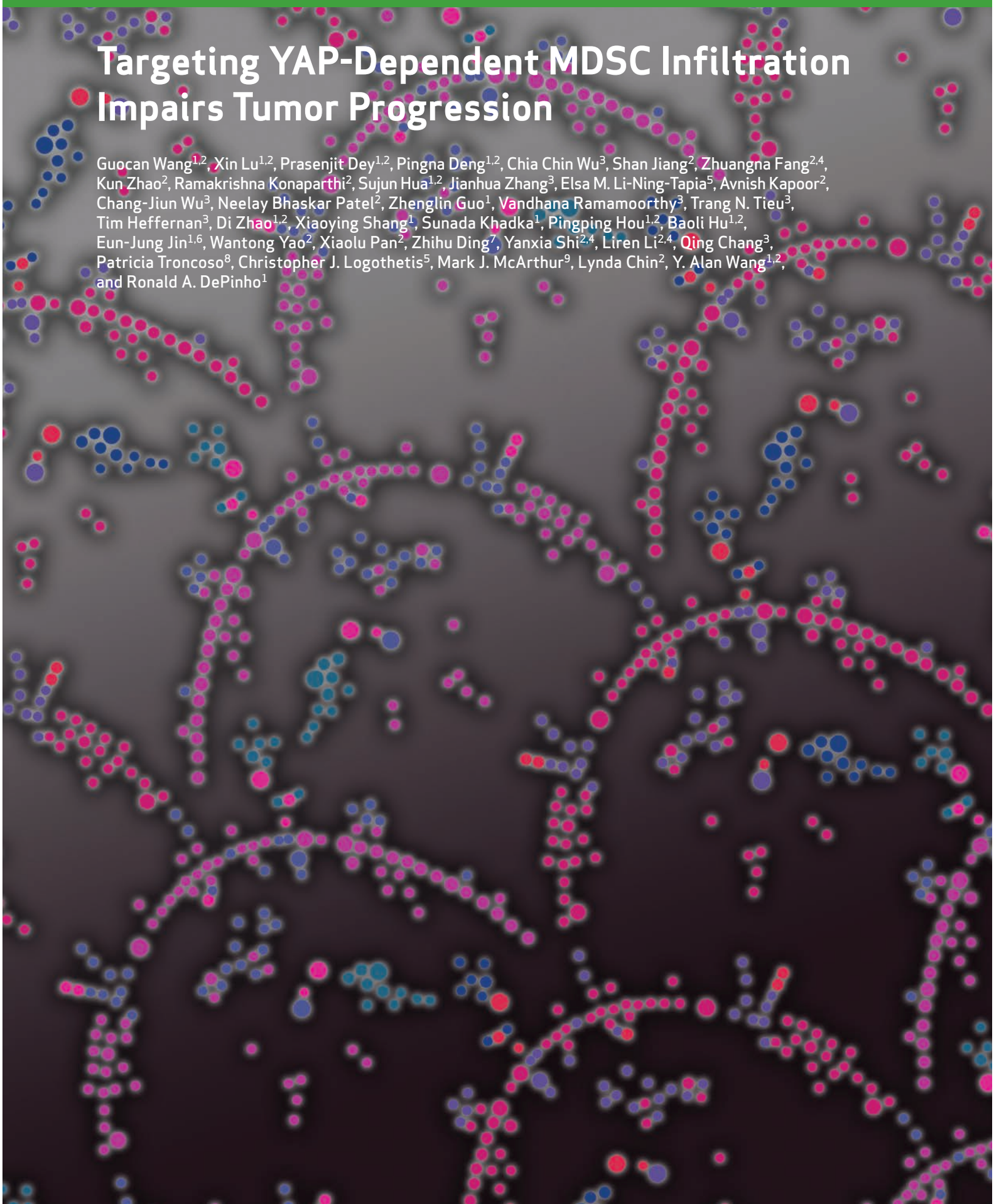

Published OnlineFirst December 23, 2015; DOI: 10.1158/2159-8290.CD-15-0224

ABSTRACT The signaling mechanisms between prostate cancer cells and infiltrating immune cells may illuminate novel therapeutic approaches. Here, utilizing a prostate adenocarcinoma model driven by loss of *Pten* and *Smad4*, we identify polymorphonuclear myeloid-derived suppressor cells (MDSC) as the major infiltrating immune cell type, and depletion of MDSCs blocks progression. Employing a novel dual reporter prostate cancer model, epithelial and stromal transcriptomic profiling identified CXCL5 as a cancer-secreted chemokine to attract CXCR2-expressing MDSCs, and, correspondingly, pharmacologic inhibition of CXCR2 impeded tumor progression. Integrated analyses identified hyperactivated Hippo–YAP signaling in driving CXCL5 upregulation in cancer cells through the YAP–TEAD complex and promoting MDSC recruitment. Clinicopathologic studies reveal upregulation and activation of YAP1 in a subset of human prostate tumors, and the YAP1 signature is enriched in primary prostate tumor samples with stronger expression of MDSC-relevant genes. Together, YAP-driven MDSC recruitment via heterotypic CXCL5–CXCR2 signaling reveals an effective therapeutic strategy for advanced prostate cancer.

SIGNIFICANCE: We demonstrate a critical role of MDSCs in prostate tumor progression and discover a cancer cell nonautonomous function of the Hippo–YAP pathway in regulation of CXCL5, a ligand for CXCR2-expressing MDSCs. Pharmacologic elimination of MDSCs or blocking the heterotypic CXCL5–CXCR2 signaling circuit elicits robust antitumor responses and prolongs survival. *Cancer Discov; 6(1); 80–95. ©2015 AACR.*

INTRODUCTION

The tumor microenvironment (TME) is comprised of a complex mixture of tumor-associated fibroblasts, infiltrating immune cells, endothelial cells, extracellular matrix proteins, and signaling molecules, such as cytokines (1–3). Homotypic and heterotypic interactions between these cellular constituents play essential roles in cancer development and response to therapeutics (3, 4). Among the infiltrating immune cells, myeloid-derived suppressor cells (MDSC) represent a phenotypically heterogeneous population of immature myeloid cells that play a tumor-promoting role by maintaining a state of immunologic anergy and tolerance (5). In particular, activated MDSCs provide a source of secreted chemokines, cytokines, and enzymes, which suppress local T-cell activation and viability (5). In addition, MDSCs can suppress T-cell activity through deprivation of nutrients, such as L-arginine and L-cysteine, and interference with T-cell receptor functions via reactive oxygen species (ROS) and reactive nitrogen species.

Prostate cancer is the most common noncutaneous malignancy in men in the United States. Similar to many other solid tumor types, prostate cancer is characterized by a rich tumor–stroma interaction network that forms the TME (1–3). In prostate cancer, various signaling pathways have been implicated in the cross-talk between tumor and stroma, such as androgen receptor signaling, FGF, SRC, TGFβ, IGF, integrin, and Hedgehog pathways (1). Interestingly, MDSC abundance in the blood correlates with circulating PSA levels in patients with prostate cancer (6–8). MDSCs have been identified recently as a TME constituent in an indolent prostate cancer mouse model with conditional *Pten* deletion (9) and demonstrated to antagonize senescence during early tumorigenesis (10). However, the molecular mechanisms underlying the recruitment of MDSCs are not well understood, and the extent to which MDSCs facilitate prostate cancer progression has not been determined.

Previously, we have shown that deletion of *Pten* in the mouse prostate causes upregulation of SMAD4, which constrains cell proliferation and invasion, and, accordingly, dual deletion of *Pten* and *Smad4* results in rapid prostate cancer progression, including metastasis (11). Comparative transcriptomic and cell profile analyses of PTEN- versus PTEN/SMAD4–deficient prostate cancer revealed a prominent immune signature and resident MDSCs as a major TME population in PTEN/SMAD4–deficient tumors. Biologic, molecular, and pharmacologic analyses established that a YAP1-mediated CXCL5–CXCR2 signaling axis recruits MDSCs into the TME and that

[1]Department of Cancer Biology, The University of Texas MD Anderson Cancer Center, Houston, Texas. [2]Department of Genomic Medicine, The University of Texas MD Anderson Cancer Center, Houston, Texas. [3]Institute for Applied Cancer Science, The University of Texas MD Anderson Cancer Center, Houston, Texas. [4]Sun Yat-Sen University Cancer Center, Guangzhou, People's Republic of China. [5]Department of Genitourinary Medical Oncology, The University of Texas MD Anderson Cancer Center, Houston, Texas. [6]Department of Biological Science, College of Natural Sciences, Wonkwang University, Cheonbuk, Iksan, South Korea. [7]Sanofi Oncology, Cambridge, Massachusetts. [8]Department of Pathology, The University of Texas MD Anderson Cancer Center, Houston, Texas. [9]Department of Veterinary Medicine and Surgery, The University of Texas MD Anderson Cancer Center, Houston, Texas.

Note: Supplementary data for this article are available at Cancer Discovery Online (http://cancerdiscovery.aacrjournals.org/).

G. Wang and X. Lu contributed equally to this article.

Corresponding Authors: Y. Alan Wang, The University of Texas MD Anderson Cancer Center, 1515 Holcombe Boulevard, Houston, TX 77030. Phone: 713-792-7928; Fax: 713-794-4005; E-mail: yalanwang@mdanderson.org; and Ronald A. DePinho, Phone: 713-792-6000, rdepinho@mdanderson.org

doi: 10.1158/2159-8290.CD-15-0224

Published OnlineFirst December 23, 2015; DOI: 10.1158/2159-8290.CD-15-0224

MDSCs play critical roles in facilitating tumor progression. Our comprehensive analyses using a prostate cancer model coupled with clinical validation using patient samples support the view that targeting either MDSC recruitment or infiltrated MDSCs may represent a valid therapeutic opportunity in treating advanced prostate cancer.

RESULTS

Prominent Infiltration of Immune Cells in the *Pten*$^{pc-/-}$*Smad4*$^{pc-/-}$ Tumor Model

We previously reported that conditional deletion of *Smad4* bypassed the senescence barrier instigated by *Pten* loss in the prostate epithelia, resulting in a highly proliferative and invasive prostate adenocarcinoma characterized by an exuberant stromal reaction and frequent metastasis to distant organs (11). Correspondingly, ingenuity pathway analysis (IPA) revealed prominent representation of cell movement, cell proliferation, and antigen presentation as the top three categories represented in the *Pten*$^{pc-/-}$*Smad4*$^{pc-/-}$ tumors (11). Further analysis revealed a prominent immune signature, including Granulocytes Adhesion and Diapedesis, Leukocytes Extravasation Signaling, and Agrandulocytes Adhesion and Diapedesis as three of the top four most activated pathways in *Pten*$^{pc-/-}$*Smad4*$^{pc-/-}$ tumors compared with those present in *Pten*$^{pc-/-}$ tumors (Fig. 1A; *P* value < 2.03E−7). Correspondingly, IHC staining highlighted conspicuous infiltration of CD45$^+$ leukocytes in *Pten*$^{pc-/-}$*Smad4*$^{pc-/-}$ tumors (Fig. 1B). To comprehensively audit the spectrum of infiltrating immune cells in tumors, we performed mass cytometry (CyTOF) immunophenotyping (12) to catalog tumor cell–type constituents from well-established tumors in 16-week-old *Pten*$^{pc-/-}$ and *Pten*$^{pc-/-}$*Smad4*$^{pc-/-}$ mice. Employing a 9-marker antibody panel (Supplementary Table S1), CyTOF confirmed a significant increase in CD45$^+$-infiltrating leukocytes in *Pten*$^{pc-/-}$*Smad4*$^{pc-/-}$ as compared with *Pten*$^{pc-/-}$ tumors (Fig. 1C). Within the CD45$^+$-infiltrating cells, CD11b$^+$ myeloid cells represented a significantly increased immune population in *Pten*$^{pc-/-}$*Smad4*$^{pc-/-}$ as compared with *Pten*$^{pc-/-}$ tumors (Fig. 1D).

CD11b$^+$Gr1$^+$ Cells Are Significantly Increased in *Pten*$^{pc-/-}$*Smad4*$^{pc-/-}$ Tumor Model

To obtain a dynamic view of peripheral and infiltrating immune cells as a function of tumor progression in the *Pten*$^{pc-/-}$*Smad4*$^{pc-/-}$ model, which initiates tumor development at 6 to 8 weeks and progresses to early invasive carcinoma by 14 weeks of age, serial CyTOF analyses using an expanded antibody panel of 17 surface markers (Supplementary Table S1) were performed on single cells from primary tumors, peripheral blood, spleen, and draining lymph nodes at 5, 8, and 14 weeks of age. The detailed immunophenotyping profiles enabled construction of the spanning-tree progression analysis of density-normalized events (SPADE)–derived tree (12). SPADE is a computational approach to facilitate the identification and analysis of heterogeneous cell types. SPADE of the *Pten*$^{pc-/-}$*Smad4*$^{pc-/-}$ model displays the complexity of the TME, which is composed of epithelial tumor cells (EpCAM$^+$CD45$^-$), nonimmune TME cells (EpCAM$^-$CD45$^-$), and infiltrating immune cells (EpCAM$^-$CD45$^+$) that can be further grouped into various immune cell subpopulations (Fig. 2A and Supplementary Fig. S1A). Among the infiltrating immune cells, there was a striking age-dependent increase of CD11b$^+$Gr1$^+$ cells in tumors (Fig. 2B) and peripheral blood from *Pten*$^{pc-/-}$*Smad4*$^{pc-/-}$ mice (Fig. 2C); this trend was much less pronounced in the spleen or draining lymph nodes (Supplementary Fig. S1B; for gating strategy, see Supplementary Fig. S1C).

CD11b$^+$Gr1$^+$ Cells from *Pten*$^{pc-/-}$*Smad4*$^{pc-/-}$ Tumors Are Potently Immunosuppressive

To evaluate the potential immunosuppressive activity of intratumoral CD11b$^+$Gr1$^+$ cells from *Pten*$^{pc-/-}$*Smad4*$^{pc-/-}$ tumors, we examined T-cell proliferation using a standard cell coculture system. These CD11b$^+$Gr1$^+$ cells strongly suppressed CD3 and CD28 antibody-induced T-cell proliferation and activation (Fig. 3A and B; see Supplementary Fig. S2 for cell isolation strategy), establishing that CD11b$^+$Gr1$^+$ cells are indeed functional MDSCs.

MDSCs can be further classified as a Ly6G$^+$Ly6C^{lo} subset with polymorphonuclear phenotype (PMN-MDSC) and a Ly6G$^-$Ly6C^{hi} subset with monocytic phenotype (M-MDSC; ref. 13). PMN-MDSCs represented the major MDSC population in *Pten*$^{pc-/-}$*Smad4*$^{pc-/-}$ tumors (Fig. 3C and D), consistent with previously observed preferential expansion of PMN-MDSCs in tumor-bearing mice of various syngeneic models (5, 9, 13). The abundance of PMN-MDSCs was further confirmed by IHC for Ly6G, as shown by quantification of both intraepithelial and stromal Ly6G$^+$ cells in tumors from *Pten*$^{pc-/-}$*Smad4*$^{pc-/-}$ mice and *Pten*$^{pc-/-}$ mice (Fig. 3E and F). It has been shown previously that ROS production by PMN-MDSCs is one of the mechanisms driving immune suppression (5, 14–16). Correspondingly, IPA revealed that pathways involved in ROS and nitric oxide (NO) production are among the top pathways activated in *Pten*$^{pc-/-}$*Smad4*$^{pc-/-}$ tumors (Fig. 1A, arrow). Consistent with the increased infiltration of PMN-MDSCs in the *Pten*$^{pc-/-}$*Smad4*$^{pc-/-}$ tumors, the expression of several subunits of NADPH oxidase (*Nox2*, *p40*^{phox}, and *p47*^{phox}), which are responsible for ROS production in PMN-MDSCs (5), was significantly upregulated in *Pten*$^{pc-/-}$*Smad4*$^{pc-/-}$ tumors relative to *Pten*$^{pc-/-}$ tumors (Fig. 3G). Moreover, *Arg1*, but not *Nos2*, was highly upregulated in the *Pten*$^{pc-/-}$*Smad4*$^{pc-/-}$ tumors (Fig. 3G). Together, MDSCs in autochthonous *Pten*$^{pc-/-}$*Smad4*$^{pc-/-}$ tumors display strong T-cell–suppressive activity and are predominantly the PMN-MDSC subtype.

Immunodepletion of MDSCs Impedes Tumor Progression in *Pten*$^{pc-/-}$*Smad4*$^{pc-/-}$ Mice

Enrichment of MDSCs in advanced *Pten*$^{pc-/-}$*Smad4*$^{pc-/-}$ tumors prompted us to explore the possible role of MDSCs in tumor progression. Using a well-characterized anti-Gr1 neutralizing monoclonal antibody (clone RB6-8C5; ref. 17), MDSCs were depleted in *Pten*$^{pc-/-}$*Smad4*$^{pc-/-}$ mice at 14 weeks of age, a point coincident with progression to the early invasive carcinoma stage (see Supplementary Fig. S3A for treatment scheme). The potent MDSC depletion activity of anti-Gr1 monoclonal antibody was evidenced by significantly decreased PMN-MDSCs and M-MDSCs in peripheral blood as early as day 2 after treatment (Supplementary Fig. S3B). In

Published OnlineFirst December 23, 2015; DOI: 10.1158/2159-8290.CD-15-0224

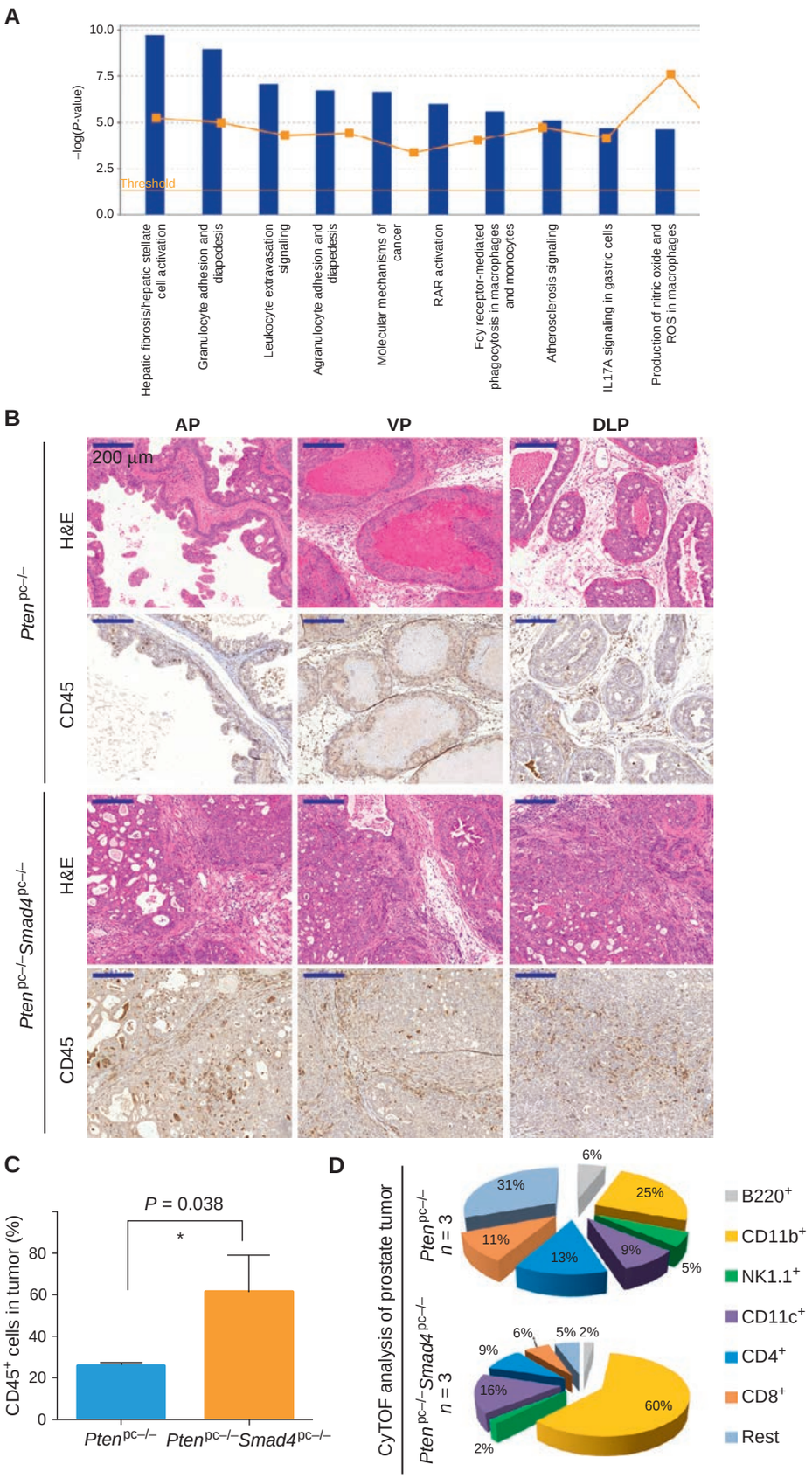

Figure 1. Prominent infiltration of immune cells in the *Pten*$^{pc-/-}$*Smad4*$^{pc-/-}$ tumors as compared with *Pten*$^{pc-/-}$ tumors. **A,** the top 10 activated pathways in *Pten*$^{pc-/-}$*Smad4*$^{pc-/-}$ tumors ($n = 5$) as compared with *Pten*$^{pc-/-}$ tumors ($n = 5$) identified by IPA. RAR, retinoic acid receptor. **B,** a significant increase in the infiltration of immune cells as shown by IHC for CD45 in *Pten*$^{pc-/-}$*Smad4*$^{pc-/-}$ tumors as compared with *Pten*$^{pc-/-}$ tumors from 16-week-old mice ($n = 3$). AP, anterior prostate; VP, ventral prostate; DLP, dorsolateral prostate; H&E, hematoxylin and eosin staining. Scale bars, 200 μm. **C,** quantification of tumor-infiltrating CD45$^+$ cells (AP, VP, and DLP combined) in *Pten*$^{pc-/-}$ tumors and *Pten*$^{pc-/-}$*Smad4*$^{pc-/-}$ from 16-week-old mice ($n = 3$), assessed by CyTOF. **D,** percentages of various immune cell populations within the CD45$^+$-infiltrating immune cells in prostate tumors from 16-week-old *Pten*$^{pc-/-}$ and *Pten*$^{pc-/-}$*Smad4*$^{pc-/-}$ mice, assessed with CyTOF (9-marker) and analyzed with FlowJo. CD11b$^+$ myeloid cells are significantly greater in *Pten*$^{pc-/-}$*Smad4*$^{pc-/-}$ tumors as compared with *Pten*$^{pc-/-}$ tumors ($n = 3$; $P < 0.05$).

Published OnlineFirst December 23, 2015; DOI: 10.1158/2159-8290.CD-15-0224

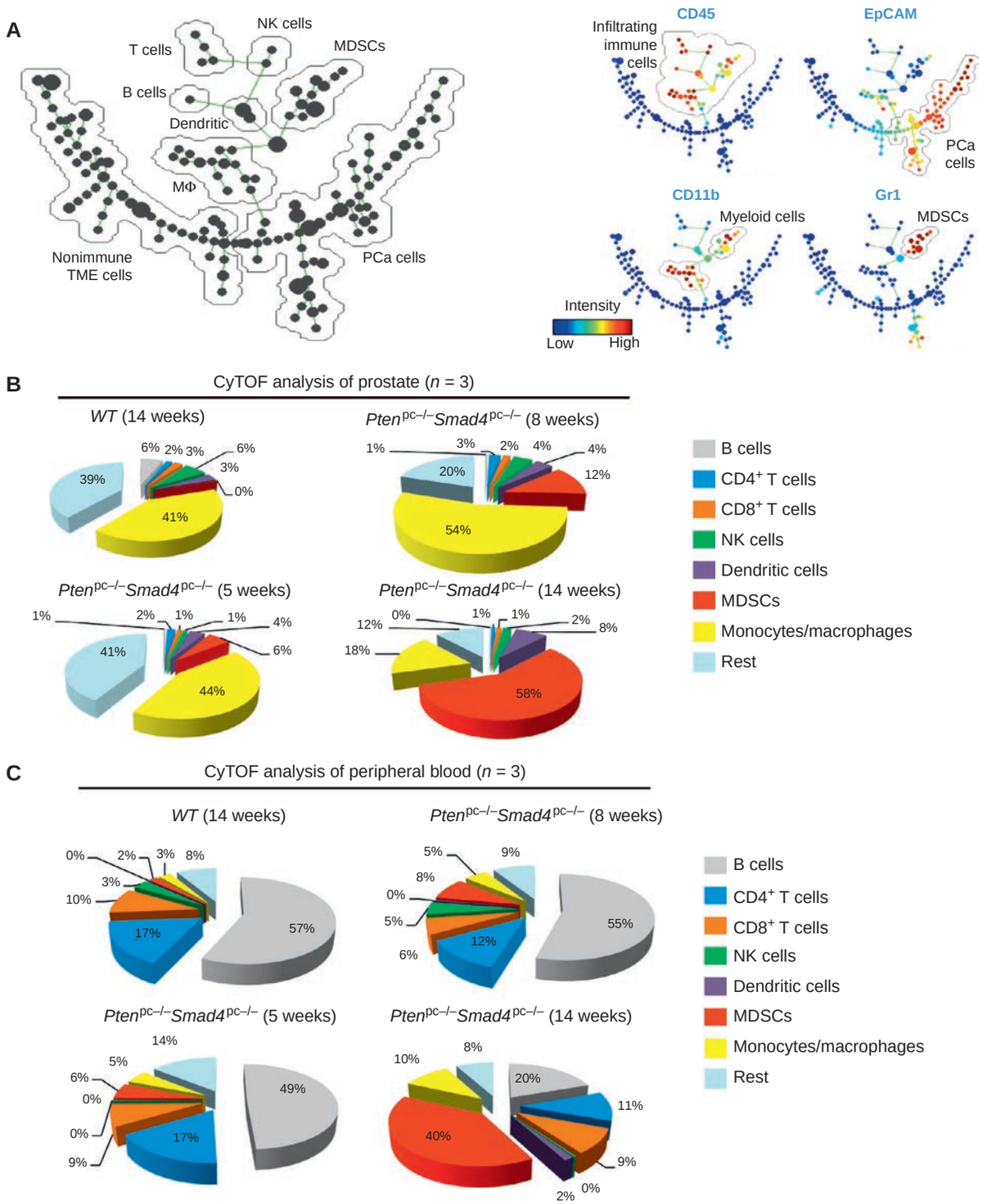

Figure 2. CD11b$^+$Gr1$^+$ cells are significantly increased in *Pten*$^{pc-/-}$*Smad4*$^{pc-/-}$ tumors as compared with *Pten*$^{pc-/-}$ tumors. **A,** SPADE tree derived from CyTOF (17-marker) analysis of whole-tumor cell population from *Pten*$^{pc-/-}$*Smad4*$^{pc-/-}$ mice at 5 weeks, 8 weeks, and 14 weeks of age ($n = 3$). Live single cells were used to construct the tree. Cell populations were identified as prostate cancer (PCa) cells (EpCAM$^+$CD45$^-$), nonimmune TME cells (EpCAM$^-$CD45$^-$), T cells (CD45$^+$CD3$^+$TCRβ$^+$), B cells (CD45$^+$B220$^+$CD19$^+$), natural killer (NK) cells (CD45$^+$NK1.1$^+$), dendritic cells (CD45$^+$CD11c$^+$), putative MDSCs (CD45$^+$CD11b$^+$Gr1$^+$), and macrophages (CD45$^+$CD11b$^+$Gr1$^-$). On the right plots, the tree is colored by the median intensity of individual markers shown on the top to highlight infiltrating immune cells (EpCAM$^-$CD45$^+$), epithelial prostate cancer cells (EpCAM$^+$CD45$^-$), total myeloid cells (CD45$^+$CD11b$^+$), and putative MDSCs (CD45$^+$CD11b$^+$Gr1$^+$). **B** and **C,** CyTOF analysis of tumors (**B**) or peripheral blood (**C**) from 5-, 8-, and 14-week-old *Pten*$^{pc-/-}$*Smad4*$^{pc-/-}$ mice revealed an age-dependent increase in the MDSC infiltration. Prostate from wild-type (WT) mice at 16 weeks old was used as control ($n = 3$ for each genotype). See also Supplementary Fig. S1.

Published OnlineFirst December 23, 2015; DOI: 10.1158/2159-8290.CD-15-0224

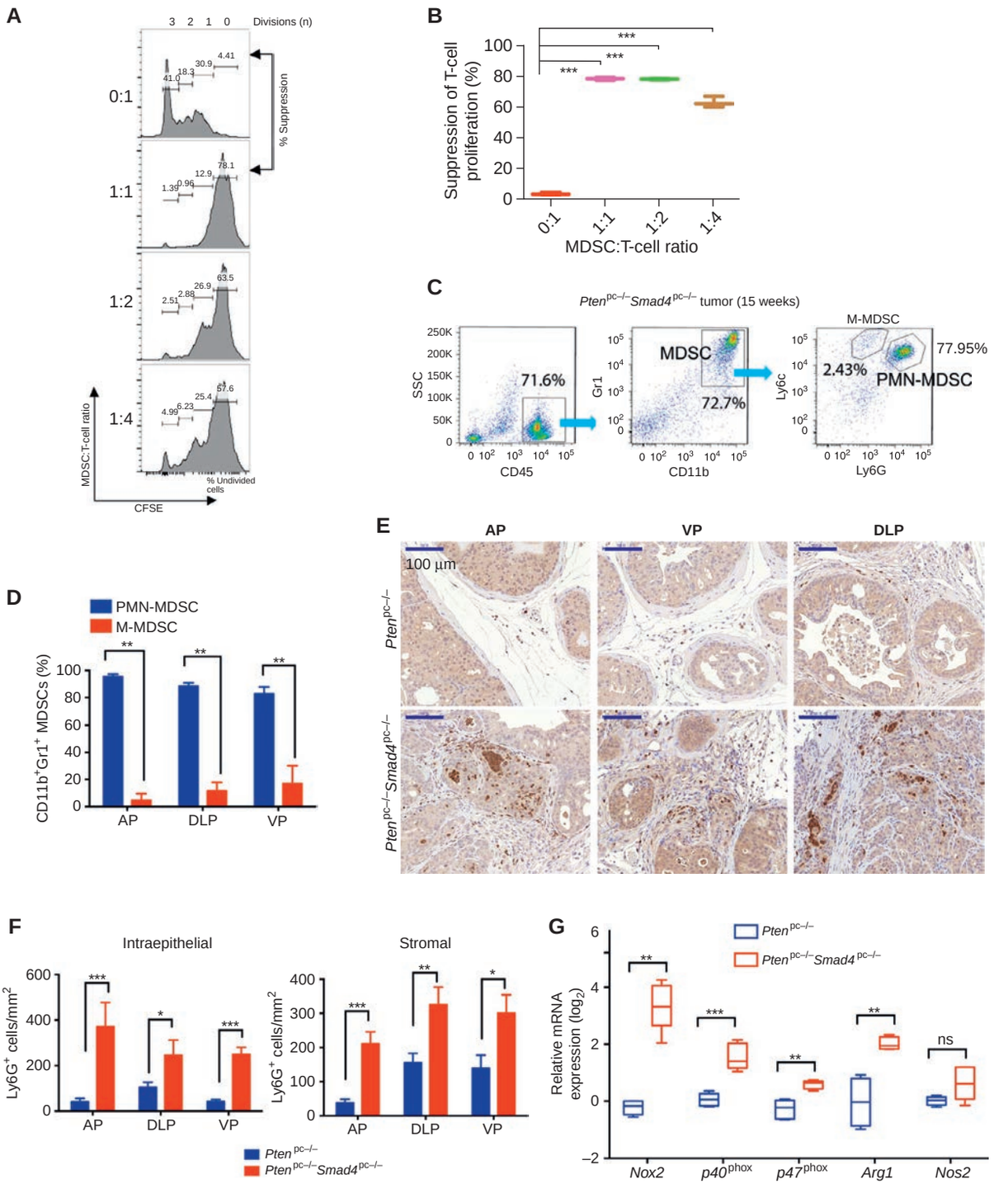

Figure 3. MDSCs from *Pten*$^{pc-/-}$*Smad4*$^{pc-/-}$ tumors display potent immunosuppressive activities and are dominated by PMN-MDSCs. **A,** CD11b^{+}Gr1^{+} cells from *Pten*$^{pc-/-}$*Smad4*$^{pc-/-}$ tumors display potent immune-suppressive activity toward T-cell activation as demonstrated by CFSE dilution assay in triplicate. **B,** summarized result from **A**. **C** and **D,** flow cytometry analysis shows PMN-MDSCs as the major population in the infiltrated MDSCs in established *Pten*$^{pc-/-}$*Smad4*$^{pc-/-}$ tumors at AP, DLP, and VP ($n = 5$). SSC, side scatter. **E** and **F,** a significant increase in Ly6G^{+} cells in *Pten*$^{pc-/-}$*Smad4*$^{pc-/-}$ tumors as compared with the *Pten*$^{pc-/-}$ tumors as shown by IHC for Ly6G and quantified by location of positively stained cells in the intraepithelial or stromal compartment of the tumor at AP, DLP, and VP ($n = 3$). **G,** quantification of the mRNA expression of subunits of NADPH oxidase (*Nox2*, *p40*^{phox}, and *p47*^{phox}), *Arg1*, and *Nos2* in the *Pten*$^{pc-/-}$*Smad4*$^{pc-/-}$ tumors and the *Pten*$^{pc-/-}$ tumors ($n = 5$). In **B, D, F,** and **G,** *, $P < 0.05$; **, $P < 0.01$; ***, $P < 0.001$; ns, nonsignificant. Also see Supplementary Fig. S2.

Published OnlineFirst December 23, 2015; DOI: 10.1158/2159-8290.CD-15-0224

addition, a systemic reduction of MDSCs in spleen, bone marrow, and prostate tumors was documented following a 30-day treatment regimen of anti-Gr1 monoclonal antibody (Fig. 4A and Supplementary Fig. S3C). This MDSC depletion was accompanied by an increase of $CD8^+$ T cells (so-called killer T cells; Fig. 4A), consistent with elimination of the T-cell suppression activity of MDSCs. Importantly, in line with the $CD8^+$ T-cell expansion, we observed that the Gr1-treated prostate displayed remarkable weight reduction in ventral and dorsolateral prostates (VP and DLP; Fig. 4B). The lack of difference in the weight of the anterior prostate (AP) is likely due to the fact that the AP tends to develop cysts with fluid accumulated inside the gland (18, 19), which also prevents the accurate measure of the prostate weight (Supplementary Fig. S3D). Histopathologic analysis revealed adenocarcinoma was the predominant pathology in mice treated with the control IgG, whereas mouse prostatic intraepithelial neoplasia (mPIN) was the predominant morphologic presentation in prostates from mice treated with anti-Gr1 monoclonal antibody (Fig. 4C and Supplementary Table S2). In addition, by immunohistochemical staining for CD45, Ki67, vimentin, smooth muscle actin (SMA), and Trichrome staining, we observed that tumor remnants in mice treated with anti-Gr1 monoclonal antibody displayed markedly reduced levels of cellular proliferation, stromal reaction, and inflammation as compared with those tumors treated with control IgG antibody (Supplementary Fig. S4A).

In another therapeutic trial, we also utilized the recently developed MDSC-specific peptide–Fc fusion protein (i.e., peptibodies) that has been shown to effectively eliminate MDSCs *in vivo* through targeting the S100A9 surface protein (20). Employing a hydrodynamic injection approach for nucleic acid delivery (21), intravenous injection of either Pep-H6 peptibody expression vector or irrelevant control peptibody vector was initiated at 14 weeks every 4 days in *Pten*$^{pc-/-}$*Smad4*$^{pc-/-}$ mice. Strikingly, a single injection of the Pep-H6 peptibody significantly reduced the MDSCs in the peripheral blood, whereas such effect was not observed using the irrelevant control peptibody (Supplementary Fig. S4B). Pep-H6 peptibody treatment for 1 month led to a dramatic decrease in cancer cell content in the prostate tumors (Fig. 4D) and provided significant survival benefit for tumor-bearing mice (Fig. 4E). Together, our data strongly support the view that MDSC depletion blocks prostate tumor progression in the *Pten*$^{pc-/-}$*Smad4*$^{pc-/-}$ model.

CXCL5–CXCR2 Signaling Promotes MDSC Recruitment and CXCR2 Inhibition Delays Tumor Progression in *Pten*$^{pc-/-}$*Smad4*$^{pc-/-}$ Mice

To elucidate the cellular origins and signaling molecules governing MDSC recruitment to prostate tumors, we incorporated the *mTmG* dual fluorescence reporter allele into the *Pten*$^{pc-/-}$*Smad4*$^{pc-/-}$ model where signaling events between tumor cells and stroma can be precisely delineated. The *mTmG* allele (22) allows Cre-dependent GFP expression in prostate epithelial cells and ubiquitous tdTomato expression in all other non–Cre-expressing cells (Fig. 5A). Transcriptomic and IPA analyses of FACS-sorted GFP^+ tumor cells and $Tomato^+$ stromal cells showed distinct expression patterns by hierarchical clustering (Fig. 5A) with tumor cells enriched for pathways involved in cell adhesion molecules and tight junctions (consistent with their epithelial nature) and stromal cells displaying activation of more diverse pathways involved in chronic inflammation, such as cytokine/cytokine receptor interaction, chemokine, JAK–STAT, T-cell repector, and B-cell receptor signaling ($P < 0.01$, data not shown). This result is consistent with the immunopathologic and histopathologic analyses showing a massive infiltration of immune cells in the *Pten*$^{pc-/-}$*Smad4*$^{pc-/-}$ tumors.

Employing this new model, we sought to identify genes that were upregulated in *Pten*$^{pc-/-}$*Smad4*$^{pc-/-}$ cancer cells relative to *Pten*$^{pc-/-}$ cancer cells that might illuminate mechanisms involved in the recruitment of MDSCs by classifying the upregulated genes into either stroma- or tumor-enriched genes. To this end, our previously generated list of 242 genes with greater than 2-fold increased expression in *Pten*$^{pc-/-}$*Smad4*$^{pc-/-}$ relative to *Pten*$^{pc-/-}$ tumors (11) was intersected with 486 genes preferentially expressed in *Pten*$^{pc-/-}$*Smad4*$^{pc-/-}$ GFP^+ cancer cells relative to $Tomato^+$ stroma cells (fold change ≥4; Supplementary Tables S3 and S4), yielding 28 genes that are markedly enriched in *Pten*$^{pc-/-}$*Smad4*$^{pc-/-}$ cancer cells (Supplementary Table S5). Among these 28 genes, *Cxcl5*, which encodes a key cytokine involved in MDSC recruitment (23, 24), is the most significantly upregulated cancer cell–specific cytokine in *Pten*$^{pc-/-}$*Smad4*$^{pc-/-}$ tumors as compared with *Pten*$^{pc-/-}$ tumors (Fig. 5B and Supplementary Fig. S5A). Notably, CXCR2, the cognate receptor for CXCL5, is also upregulated in *Pten*$^{pc-/-}$*Smad4*$^{pc-/-}$ tumors as compared with *Pten*$^{pc-/-}$ tumors and is significantly enriched in *Pten*$^{pc-/-}$*Smad4*$^{pc-/-}$ $Tomato^+$ stroma cells (Fig. 5B). The upregulation of CXCL5 expression in *Pten*$^{pc-/-}$*Smad4*$^{pc-/-}$ prostate tumors was further confirmed by IHC (Fig. 5C). In addition, we performed FACS analysis of $CD11b^+Gr1^+$ cells and $CD11b^-Gr1^-$ cells from bone marrow, spleen, peripheral blood, and tumors for CXCR2 expression. As shown in Supplementary Fig. S5B, $CD11b^-Gr1^-$ cells (largely lymphocytes) are devoid of CXCR2 expression, whereas a large fraction of $CD11b^+Gr1^+$ cells express CXCR2. When CXCR2 expression was further separated into $CXCR2^{hi}$ and $CXCR2^+$, we observed an enrichment of the $CXCR2^{hi}$ subpopulation in the $CD11b^+Gr1^+$ cells in prostate tumors compared with $CD11b^+Gr1^+$ cells from bone marrow, spleen, or blood (Supplementary Fig. S5B). This is consistent with the model of active recruitment of MDSCs by tumors through CXCR2-mediated chemoattraction.

To validate the CXCL5–CXCR2 axis in the recruitment of MDSCs to the TME of *Pten*$^{pc-/-}$*Smad4*$^{pc-/-}$ tumors, we assessed the impact of pharmacologic inhibition of CXCL5 and CXCR2 in MDSCs using a transwell migration assay (23). First, anti–CXCL5-neutralizing antibody pretreatment of conditioned medium (CM) derived from *Pten*$^{pc-/-}$*Smad4*$^{pc-/-}$ prostate cancer cell line resulted in decreased migration of MDSCs (Fig. 5D). Second, CXCR2 inhibitor SB255002 or anti-CXCR2 neutralizing antibody pretreatment also impeded migration of MDSCs (Fig. 5D). Third, *in vivo* blockade of the CXCL5–CXCR2 axis using SB255002 in 14-week-old *Pten*$^{pc-/-}$*Smad4*$^{pc-/-}$ mice over a 14-day daily dosing schedule revealed a dramatic reduction in infiltration of MDSCs in the prostate tumors (Supplementary Fig. S5C and S5D). Notably, similar to mice treated with anti-Gr1 neutralizing antibody, these SB225002-treated *Pten*$^{pc-/-}$*Smad4*$^{pc-/-}$ mice also showed significant reduction in tumor burden (VP and DLP) as compared with the vehicle-treated controls (Fig. 5E and Supplementary Fig. S5E). Strikingly,

Published OnlineFirst December 23, 2015; DOI: 10.1158/2159-8290.CD-15-0224

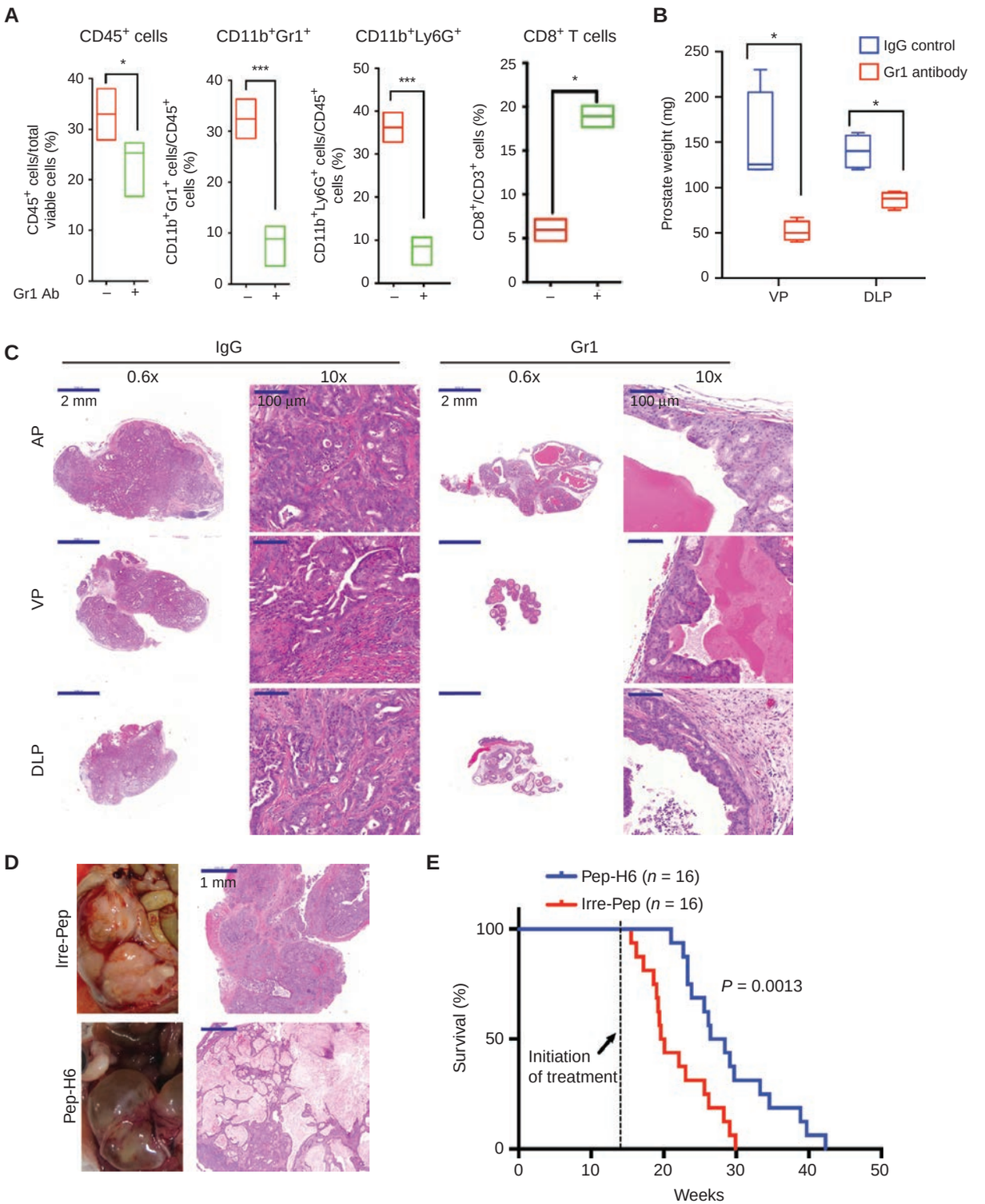

Figure 4. Targeting MDSCs with anti-Gr1 neutralizing antibody or MDSC-specific peptibody significantly delayed tumor progression in *Pten*$^{pc-/-}$*Smad4*$^{pc-/-}$ mice. **A,** administration of Gr1-neutralizing antibody *in vivo* significantly reduced CD45$^+$-infiltrating immune cells, reduced MDSCs, and increased CD8$^+$ T cells among total T cells in *Pten*$^{pc-/-}$*Smad4*$^{pc-/-}$ tumors ($n = 4$), measured by flow cytometry. **B,** Gr1 antibody treatment of 14-week-old mice significantly reduced the weight of VP and DLP in *Pten*$^{pc-/-}$*Smad4*$^{pc-/-}$ mice. **C,** Gr1 antibody remarkably altered the tumor histopathology in *Pten*$^{pc-/-}$*Smad4*$^{pc-/-}$ adenocarcinoma, analyzed by hematoxylin and eosin staining of AP, VP, and DLP. **D,** one month of Pep-H6 peptibody treatment led to significant appearance and histology changes of the *Pten*$^{pc-/-}$*Smad4*$^{pc-/-}$ adenocarcinoma. Irre-Pep, irrelevant control peptibody. **E,** Kaplan–Meier survival curve showing the significant delay of mortality caused by Pep-H6 peptibody treatment of *Pten*$^{pc-/-}$*Smad4*$^{pc-/-}$ mice. In **A** and **B,** *, $P < 0.05$ and ***, $P < 0.001$; Also see Supplementary Figs. S3 and S4.

Published OnlineFirst December 23, 2015; DOI: 10.1158/2159-8290.CD-15-0224

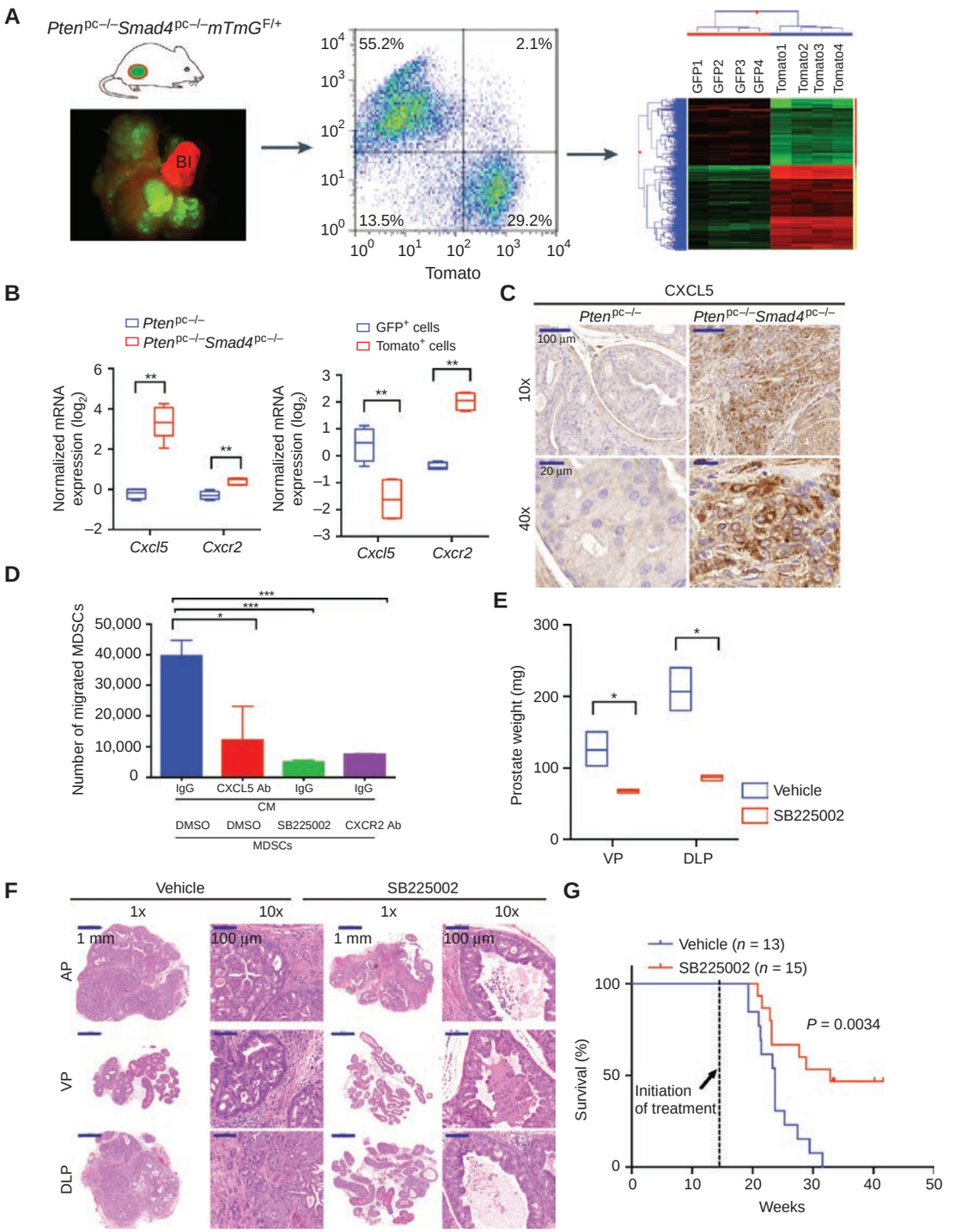

Figure 5. CXCL5–CXCR2 axis plays an indispensable role in recruitment of MDSCs and promotion of tumor progression. **A,** establishment of *Pten*$^{pc-/-}$*Smad4*$^{pc-/-}$*mTmG*$^{+}$ model allows fluorescent visualization of the GFP^{+} tumor cells intermixed with Tomato^{+} stroma (left; FACS isolation of GFP^{+} tumor cells and Tomato^{+} stromal cells from the prostate adenocarcinoma (middle); microarray analysis to identify differentially expressed genes (right). In the fluorescence image, Bl denotes bladder (completely Tomato^{+}; $n = 2$). **B,** quantification of mRNA expression shows that *Cxcl5* and *Cxcr2* were both expressed at higher levels in *Pten*$^{pc-/-}$*Smad4*$^{pc-/-}$ tumors than in *Pten*$^{pc-/-}$ tumors, and *Cxcl5* expression was enriched in GFP^{+} tumor cells, whereas *Cxcr2* expression was enriched in Tomato^{+} stromal cells ($n = 5$). **C,** IHC for CXCL5 showed significantly higher expression levels of CXCL5 in *Pten*$^{pc-/-}$*Smad4*$^{pc-/-}$ tumors than *Pten*$^{pc-/-}$ tumors ($n = 3$). **D,** blocking the CXCL5–CXCR2 axis by CXCL5-neutralizing antibody, CXCR2 inhibitor SB225002, or CXCR2-neutralizing antibody significantly decreased migration of MDSCs toward conditioned medium from *Pten*$^{pc-/-}$*Smad4*$^{pc-/-}$ tumor cells, evaluated with an *in vitro* transwell migration assay in triplicate. **E** and **F,** CXCR2 inhibitor SB225002 treatment of *Pten*$^{pc-/-}$*Smad4*$^{pc-/-}$ mice for 14 days ($n = 4$) resulted in significantly reduced tumor weight of VP and DLP and significantly delayed progression for AP prostate cancer shown by hematoxylin and eosin staining. **G,** CXCR2 inhibitor SB225002 treatment of *Pten*$^{pc-/-}$*Smad4*$^{pc-/-}$ mice significantly prolonged their overall survival. In **B, D,** and **E,** *, $P < 0.05$; **, $P < 0.01$; and ***, $P < 0.001$. Also see Supplementary Fig. S5.

Published OnlineFirst December 23, 2015; DOI: 10.1158/2159-8290.CD-15-0224

all SB225002-treated tumors presented with prostatic intraepithelial neoplasia (PIN) pathology, whereas the control group uniformly possessed advanced adenocarcinoma (Fig. 5F and Supplementary Table S2). Furthermore, SB225002 treatment significantly prolonged the overall survival of the *Pten*$^{pc-/-}$*Smad4*$^{pc-/-}$ mice as compared with the vehicle control (Fig. 5G). Thus, we conclude that the CXCL5–CXCR2 axis plays a prominent role in the recruitment of MDSCs to the *Pten*$^{pc-/-}$*Smad4*$^{pc-/-}$ prostate TME and that inhibition of this axis profoundly impairs tumor progression.

YAP1 Is Activated in *Pten*$^{pc-/-}$*Smad4*$^{pc-/-}$ Tumors and Directly Regulates *Cxcl5* Transcription

Having identified cancer cell–derived CXCL5 as a key signaling molecule governing recruitment of MDSCs into the TME, we sought to define the molecular mechanisms underlying the strong induction of CXCL5 expression in the *Pten*$^{pc-/-}$*Smad4*$^{pc-/-}$ cancer cells. As CXCL5 expression is not significantly upregulated in the *Pten*$^{pc-/-}$ tumors (Fig. 5C), we performed unbiased Gene Set Enrichment Analysis (GSEA) to identify pathways that were activated in the *Pten*$^{pc-/-}$*Smad4*$^{pc-/-}$ tumors as compared with *Pten*$^{pc-/-}$ tumors, aiming to identify potential regulators for *Cxcl5* in *Pten*$^{pc-/-}$*Smad4*$^{pc-/-}$ tumors. The YAP oncogenic signature emerged as the second most hyperactivated pathway (Fig. 6A and Supplementary Fig. S6A). Although it is known that the Hippo–YAP pathway plays an important role in development and cancer in organs such as the liver, skin, intestine, and pancreas (25–27), the role for the Hippo–YAP pathway in prostate cancer biology is emerging. Specifically, Hippo pathway components LATS1/2 have been implicated in anoikis and metastasis in prostate cancer (28), and ERG-induced YAP1 activation can promote age-related prostate tumor development (29). However, beyond the cancer cell–specific functions, the Hippo–YAP1 pathway has not been linked to signaling communication between cancer cells and immune cells in the TME. Consistent with the *in silico* analysis, IHC analysis documented a dramatic increase in the nuclear localization of YAP1 in *Pten*$^{pc-/-}$*Smad4*$^{pc-/-}$ cancer cells as compared with *Pten*$^{pc-/-}$ cancer cells (Fig. 6B). As YAP1, a transcriptional coactivator and the downstream mediator of Hippo signaling, is regulated posttranscriptionally by either kinase-mediated degradation or cytoplasmic sequestration (25), our findings of increased nuclear localization of YAP1 are consistent with the hypothesis that the Hippo–YAP pathway is activated in the *Pten*$^{pc-/-}$*Smad4*$^{pc-/-}$ tumors. In addition, unbiased oPOSSUM analysis (30) indicated that TEAD1, a member of the TEAD transcription factor family that is required for YAP1 function, ranked second among the top 10 transcription factors with over-represented binding sites in the 70 cancer-specific genes that were upregulated in the *Pten*$^{pc-/-}$*Smad4*$^{pc-/-}$ tumors as compared with the *Pten*$^{pc-/-}$ tumors (≥1.5 fold, Z-Score = 13.362; Supplementary Fig. S6B and S6C), an observation reinforcing the relevance of the Hippo–YAP pathway. Furthermore, we identified six YAP/TEAD binding motifs in the promoter of *Cxcl5* gene (Supplementary Fig. S6D), suggesting YAP1 could be directly involved in the recruitment of MDSCs through regulating *Cxcl5* expression. This hypothesis was supported by chromatin immunoprecipitation (ChIP) assay showing that YAP1 binds to *Cxcl5* promoter (Fig. 6C) and that shRNA-mediated knockdown of *Yap1* in *Pten*$^{pc-/-}$*Smad4*$^{pc-/-}$ cancer cells drastically reduced the expression of *Cxcl5* mRNA (Fig. 6D). In addition, overexpression of a constitutively active YAP1^{S127A} mutant dramatically increased *Cxcl5* mRNA expression in the *Pten*$^{pc-/-}$*Smad4*$^{pc-/-}$ cell line (Fig. 6E), whereas overexpression of a TEAD binding defective YAP1 mutant S127A/S94A compromised its ability to activate *Cxcl5* transcription (Fig. 6F). To examine the effect of YAP1-dependent cytokine signaling in the regulation of MDSCs recruitment, we first prepared CM from the *Pten*$^{pc-/-}$*Smad4*$^{pc-/-}$ cell line either infected with shRNA against *Yap1* or pretreated with verteporfin (25), a small-molecular inhibitor that disrupts YAP1–TEAD interaction. We then tested the effect of various CM on the migration of MDSCs *in vitro*. As shown in Fig. 6G and H, we observed significantly decreased MDSC migration *in vitro* when CM was from cells with either YAP1 knockdown or verteporfin treatment.

Finally, to test if targeting YAP1 *in vivo* can impair the infiltration of MDSCs and inhibit tumor growth, we used our recently isolated syngeneic murine prostate cancer line PPS, which is derived from the backcrossed *Pten*$^{pc-/-}$*Smad4*$^{pc-/-}$*Trp53*$^{pc-/-}$ model (31) and can form subcutaneous or orthotopic tumors robustly in C57BL/6 hosts. Doxycycline-dependent shRNA knockdown of *Yap1* (two independent shRNA designs #1 and #3) was established in PPS (Fig. 6I) and injected subcutaneously in C57BL/6 mice. YAP1 knockdown induced by switching to doxycycline-containing drinking water resulted in a reduction of MDSCs in the intratumoral CD45$^+$ population (Fig. 6J and K) and impaired tumor progression (Fig. 6L). Although the observation supports the hypothesis that targeting YAP1-dependent MDSC infiltration impairs tumor growth, we acknowledge that the tumor growth impediment by YAP1 silencing is likely due to a combined effect of both cell-nonautonomous and cell-autonomous mechanisms. Together, these findings reveal a novel function for YAP1 in the recruitment of MDSCs through direct upregulation of *Cxcl5* transcription in prostate tumor cells.

YAP1 Is Activated in Human Prostate Cancer and Tracks with an MDSC Signature

To determine whether YAP1 is overexpressed and activated in human prostate cancer, we performed IHC staining of a human prostate cancer tissue microarray (TMA) for YAP1. Interestingly, YAP1 is expressed in basal cells, but not in the luminal cells of the normal human prostate (Fig. 7A). In addition, we observed that YAP1 is overexpressed in a subset of human prostate cancers (Fig. 7A and B and Supplementary Table S6), consistent with a recent report (29). Given the lack of validated antibodies for human MDSCs for TMA analysis, we generated a list of 39 MDSC-related genes curated from literature analysis (Supplementary Table S7) to generate evidence of a link between YAP1 activation and MDSC prominence in human prostate. Using the prostate RNA-sequencing data from The Cancer Genome Atlas (TCGA), unsupervised clustering with the 39-gene MDSC signature categorized 498 TCGA primary prostate tumors into three subtypes: MDSC-high (n = 139), MDSC-medium (n = 158), and MDSC-low (n = 201; Fig. 7C), suggesting that a subset of human prostate tumors may have prominent infiltration of MDSCs. In addition, using GSEA, we found that several YAP1 signature genes are significantly overexpressed in MDSC-high samples as compared with MDSC-low samples (Fig. 7D; P value < 0.005), reinforcing the link between MDSC-high prostate tumors and YAP1 transcriptional activities. Furthermore,

Published OnlineFirst December 23, 2015; DOI: 10.1158/2159-8290.CD-15-0224

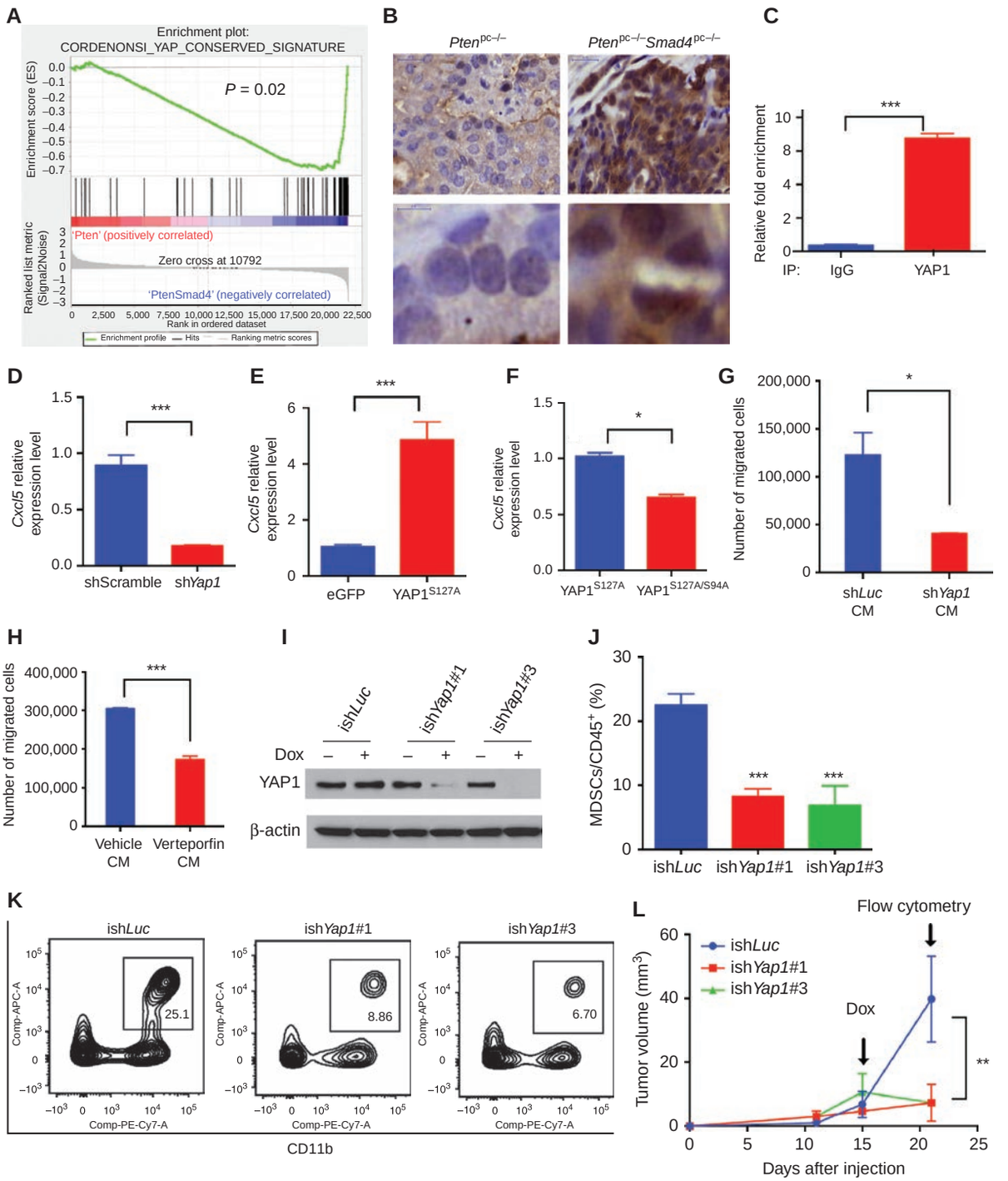

Figure 6. Hyperactivation of YAP1 in *Pten*$^{pc-/-}$*Smad4*$^{pc-/-}$ tumors upregulates *Cxcl5*. **A,** GSEA analysis identified the YAP1 oncogenic signature as the top activated pathway in the *Pten*$^{pc-/-}$*Smad4*$^{pc-/-}$ tumors compared with *Pten*$^{pc-/-}$ tumors ($n = 5$). **B,** a significant increase in nuclear staining of YAP1 in the *Pten*$^{pc-/-}$*Smad4*$^{pc-/-}$ tumors compared with *Pten*$^{pc-/-}$ tumors ($n = 3$). **C,** ChIP shows that YAP1 can directly bind to *Cxcl5* promoter using quantitative PCR in triplicates. **D,** shRNA knockdown of *Yap1* in *Pten*$^{pc-/-}$*Smad4*$^{pc-/-}$ tumor cells resulted in a dramatic reduction in *Cxcl5* mRNA expression using quantitative PCR in triplicate. **E,** overexpression of a constitutively active YAP1^{S127A} mutant resulted in upregulation of *Cxcl5* mRNA using quantitative PCR in triplicate. **F,** TEAD-binding defective YAP1$^{S127A/S94A}$ mutant significantly decreased *Cxcl5* mRNA expression as compared with the YAP1^{S127A} mutant using quantitative PCR in triplicate. **G** and **H,** conditioned medium prepared from *Pten*$^{pc-/-}$*Smad4*$^{pc-/-}$ cells infected with *Yap1* shRNA (**G**) or treated with verteporfin (**H**), a small molecule that disrupts YAP1–TEAD interaction, induced less MDSC migration *in vitro* as compared with the control conditioned medium. Transwell migration was done in triplicate for each condition. **I,** Western blot analysis showed that two independent inducible shRNAs for *Yap1* efficiently knock down *Yap1* expression in the *Pten*$^{pc-/-}$*Smad4*$^{pc-/-}$cells. **J–L,** inducible *Yap1* knockdown strongly suppressed the intratumoral MDSC infiltration (**J** and **K**) and tumor growth (**L**) of the C57BL/6-syngeneic cell line isolated from prostate tumor of *Pten*$^{pc-/-}$*Smad4*$^{pc-/-}$*Trp53*$^{pc-/-}$ mice ($n = 5$). In **C, D, E** and **F, G, H, L,** *, $P < 0.05$; **, $P < 0.01$; ***, $P < 0.001$. See also Supplementary Fig. S6.

Published OnlineFirst December 23, 2015; DOI: 10.1158/2159-8290.CD-15-0224

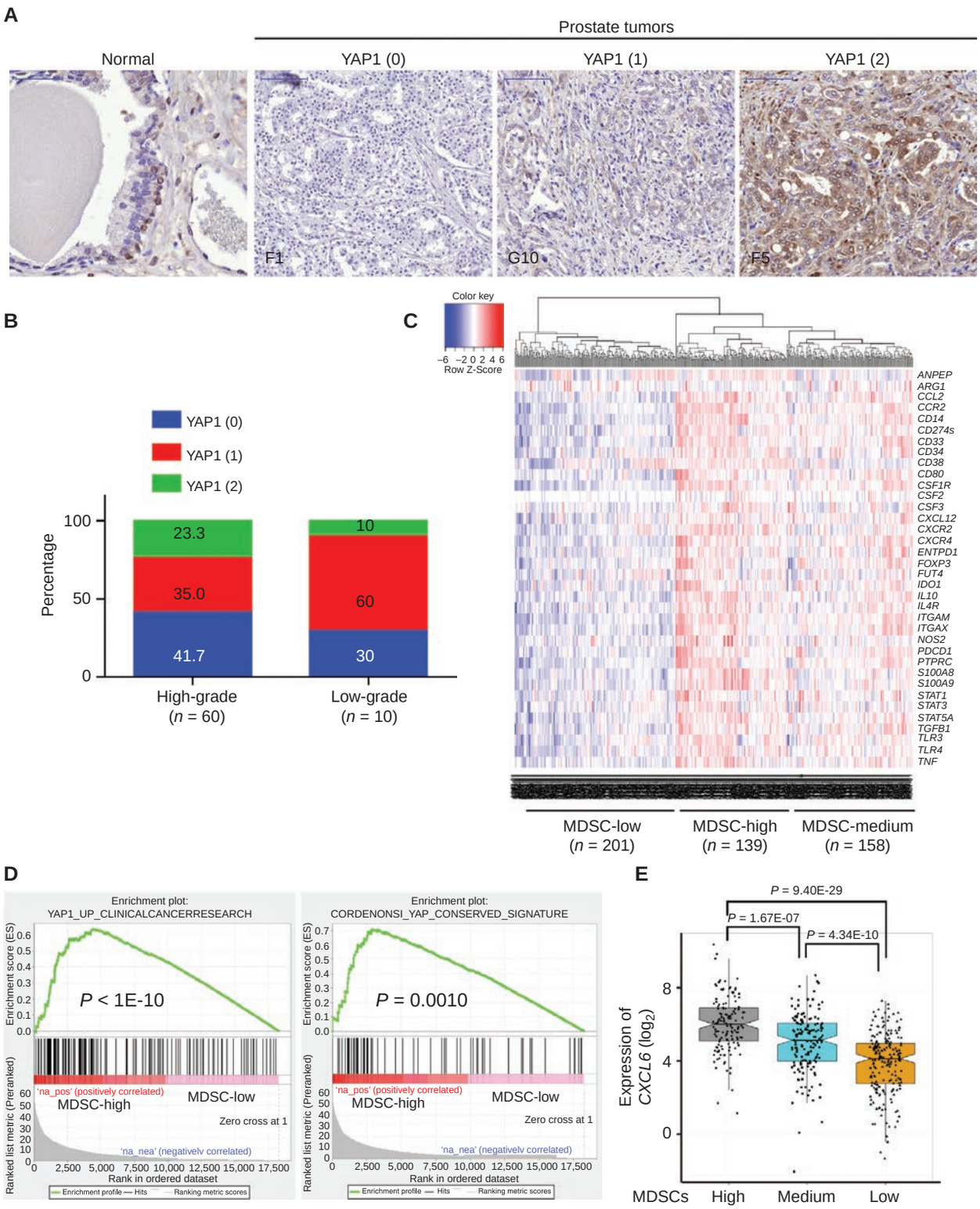

Figure 7. YAP1 is activated in human prostate cancer and correlated with MDSC signature and *CXCL6* overexpression. **A,** IHC analysis of YAP1 expression in basal cells of normal prostate tissue and human prostate cancers. Numbers in parentheses indicate YAP1 IHC intensity scores. **B,** YAP1 IHC intensity score representation in low-grade ($n = 10$) and high-grade ($n = 60$) prostate cancer. **C,** clustering of human TCGA prostate samples into MDSC-high, MDSC-low, and MDSC-medium groups using a 39-gene MDSC signature. **D,** YAP1 signatures are identified in MDSC-high prostate TCGA samples. **E,** *CXCL6* expression is significantly higher in the MDSC-high group. See also Supplementary Fig. S7.

Published OnlineFirst December 23, 2015; DOI: 10.1158/2159-8290.CD-15-0224

CXCL6, the human homolog of murine *Cxcl5*, is expressed at higher levels in the MDSC-high samples as compared with MDSC-low samples (Fig. 7E; $P = 9.40E{-}29$). Similar analysis was performed in a published dataset focused on tumor immunobiological differences in prostate cancer between African-American and European-American men (32). The 39-gene MDSC signature can cluster the 69 primary prostate tumors into MDSC-high ($n = 40$) and MDSC-low groups ($n = 29$), and YAP1 signatures were prominent in the MDSC-high groups (Supplementary Fig. S7A and S7B). Together, these human prostate tumor findings, which parallel our murine observations, suggest that activated YAP1 is integral to MDSC infiltration in both mouse and human prostate cancer, thus enhancing the translational value of the study.

DISCUSSION

Although a large number of studies have demonstrated a direct relationship between MDSC frequency and tumor burden (5), our understanding of the role of MDSCs in tumor progression, particularly prostate cancer, remains largely speculative. Here, using a highly invasive PTEN/SMAD4-deficient prostate cancer model, we established the signaling circuits involved in the recruitment of MDSCs to the TME and demonstrated a critical role of these cells in facilitating tumor progression.

Homozygous deletion of *Pten* in murine prostate elicited a strong senescence response that restricts tumor progression (33); thus, *Pten*-deficient prostate tumors are largely indolent and progress slowly to invasive prostate adenocarcinoma without metastasis to distant organs (11, 33). Recently, it was shown that infiltrating $Gr1^+$ myeloid cells suppress *Pten* loss–induced cellular senescence through a paracrine signaling mediated by myeloid-secreted IL1RA (10). We have previously reported that deletion of *Smad4* leads to bypass of *Pten* loss–induced senescence in prostate cancer progression, resulting in aggressive cancer cell proliferation and invasion/metastasis (11). Using the state-of-the-art CyTOF technology, we revealed that progression in the $Pten^{pc-/-}Smad4^{pc-/-}$ model is associated with abundant immune cell infiltration characterized by prominent representation of $CD11b^+Gr1^+$ MDSCs, which display potent immunosuppressive activities as shown by their strong antagonistic effect on T-cell proliferation (Fig. 3A and B).

The basis for the increased frequency of MDSCs in the TME and, specifically in the $Pten^{pc-/-}Smad4^{pc-/-}$ model, was not known and presumably could derive from either active chemoattraction or passive nonspecific responses to tissue stress associated with expanding tumor burden. Taking an unbiased approach to identify pathways that may recruit MDSCs, we deconvoluted cancer versus stromal cell transcriptomes by exploiting a Cre-dependent dual fluorescence lineage tracing system in the $Pten^{pc-/-}Smad4^{pc-/-}$ model. This approach identified unique immune regulatory molecules that are activated prominently in $Pten^{pc-/-}Smad4^{pc-/-}$ cancer cells, most prominently CXCL5. We established that the CXCL5 chemokine plays a key role in the efficient recruitment of MDSCs which enables tumor progression, as blocking CXCL5–CXCR2 signaling with a CXCR2 inhibitor led to reduced MDSC infiltration with associated antitumor effects. It should be noted that the human homolog for murine CXCL5 is CXCL6, and CXCL6 has been shown to be upregulated in prostate cancer as compared with normal prostate and significantly associated with high Gleason scores 8 to 9 (34). Interestingly, it was shown that CXCL5 promotes recruitment of MDSCs to primary melanoma, resulting in epithelial–mesenchymal transition (EMT) and cancer cell dissemination (35). Thus, the possible role of CXCL5/CXCL6 in prostate cancer metastasis merits further study.

Our finding that CXCL5 is the main chemoattractant in the $Pten^{pc-/-}Smad4^{pc-/-}$ model also provided a framework to determine the cancer cell signaling pathways driving *Cxcl5* upregulation. By integration of bioinformatic analysis and experimental validation, we identified that YAP1 is activated in $Pten^{pc-/-}Smad4^{pc-/-}$ prostate tumors and that YAP1 directly regulates *Cxcl5* transcription and MDSC recruitment. In addition, we showed that YAP1 is overexpressed in a subset of human prostate cancers, which is consistent with a recent publication showing a correlation of ERG and YAP1 coexpressed in a subset of human prostate cancers (29). Importantly, a 39-gene MDSC signature clusters the prostate TCGA samples into three subtypes. By comparing the samples with high and low abundance of MDSC-related gene expression, YAP1 signatures and higher expression of CXCL6 are identified in the MDSC-high samples, which is consistent with our findings in the mouse model. Furthermore, the 39-gene MDSC signature can cluster primary prostate tumor samples from a published dataset (32) into two subtypes using MDSC-high and MDSC-low, with YAP1 signatures identified in the MDSC-high subtype. The Hippo–YAP signaling pathway is widely deregulated in human solid neoplasia and often associated with enhanced cancer cell proliferation and cancer stem cell phenotypes (25), and is implicated in the regulation of anoikis and metastasis in prostate cancer (28) and the development of age-related prostate cancers driven by ERG overexpression (29), yet how the Hippo–YAP pathway regulates the TME in prostate cancer has hitherto not yet been elucidated. Our finding of a novel non–cell autonomous function for Hippo–YAP signaling in MDSC recruitment in TME complements well the recently elucidated roles of YAP1 in promoting cell-autonomous functionality of cancer cells, including enhanced tumor survival, EMT, and bypass mechanism for oncogene addiction (26, 27).

Pharmacologic depletion of MDSCs using Gr1 antibody, Pep-H6 peptibody, or CXCR2 inhibitor arrested prostate progression at the high-grade PIN stage whereas controls exhibited full-fledged adenocarcinoma in $Pten^{pc-/-}Smad4^{pc-/-}$ model. Given that treatment commences at 14 weeks of age (Supplementary Fig. S3A), when prostate tumors have uniformly advanced to the invasive adenocarcinoma stage (11) with significant MDSC infiltration (Fig. 2B), our findings support the view that anti-MDSC treatment provokes regression of advanced tumors. In addition, both Pep-H6 peptibody and CXCR2 inhibitor treatment significantly prolonged the overall survival of the $Pten^{pc-/-}Smad4^{pc-/-}$ tumor-bearing mice. Therefore, our preclinical data suggest that pharmacologic depletion of MDSCs may offer potential therapeutic benefits for patients with advanced prostate cancer, particularly those deficient for PTEN and SMAD4. In line with our findings, others have demonstrated that depletion of G-MDSCs promotes the intratumoral accumulation of activated $CD8^+$ T cells and apoptosis of tumor epithelial cells in a *Kras/Trp53* mouse pancreatic cancer model (36).

Published OnlineFirst December 23, 2015; DOI: 10.1158/2159-8290.CD-15-0224

MDSCs are of myeloid cell lineage, and their coordinated regulation represents one of the most complex aspects of cancer–host interactions (37). The involvement of the myeloid compartment of the hematopoietic system in innate immunity, adaptive immunity, as well as in regulation of TME through nonimmune mechanisms highlights the need to understand more deeply how modulating different myeloid populations, including MDSCs, can positively or negatively affect tumor growth.

Pep-H6 peptibody, targeting S100A9 expressed on MDSCs, has been shown to have minimal toxicity in treated mice (20) and potent antitumor activity (Fig. 4D and E; ref. 18). Interestingly, tasquinimod, a small-molecular inhibitor for S100A9, has been shown to increase progression-free survival and overall survival for metastatic castration-resistant prostate cancer in a phase II clinical trial and has entered phase III clinical trials (38). Importantly, similar to the peptibody treatment in mice, tasquinimod is well tolerated and causes only minor adverse effects in human patients (38), suggesting that tasquinimod or similar drugs targeting S100A9 could potentially be used as chemopreventive agents for patients with high-risk primary prostate cancer. The antiproliferative mechanism may explain why targeting CXCR2 in prostate cancer with abundant preexisting MDSC infiltration can lead to MDSC depletion, as MDSCs have been shown to undergo active proliferation inside the prostate tumor of the *Pten*$^{pc-/-}$ model (9). The effectiveness of targeting CXCR2 in our model suggests targeting mechanisms that specifically regulate MDSC recruitment as well as their proliferative and survival potential in human cancers would provide therapeutic benefit for patients with prostate cancer.

Targeting MDSCs as a cooperative approach for immunotherapy is clinically relevant, as increasing evidence indicates MDSCs represent a *bona fide* immunosuppressive cell population in patients with various solid tumors (39, 40). Immunosuppressive mechanisms by MDSCs in mice have been validated in humans, which include L-arginine depletion, NO and ROS production, TGFβ secretion, blocking T_{eff} cells and inducing T_{reg} cells, among others (39). Future studies are warranted to evaluate if combining MDSC depletion with immune checkpoint inhibitors, such as anti–CTLA-4, anti–PD-1, and anti–PD-L1 antibodies, may elicit synergistic efficacy in preclinical models of prostate cancer and eventually benefit patients with prostate cancer.

METHODS

Mice Strains

Pten$^{pc-/-}$ and *Pten*$^{pc-/-}$*Smad4*$^{pc-/-}$ models were developed previously (11) and were backcrossed to the C57BL/6 background for more than four generations. B6.129(Cg)-Gt(ROSA)26Sortm4(ACTB-tdTomato,-EGFP) Luo/J ("mTmG") strain was obtained from The Jackson Laboratory. Mice were maintained in pathogen-free conditions at the MD Anderson Cancer Center. All manipulations were approved under the MD Anderson Cancer Center Institutional Animal Care and Use Committee.

Cell Lines

Pten$^{pc-/-}$*Smad4*$^{pc-/-}$ prostate cell lines, which have been described previously (11), were generated in 2010. PPS, a C57BL/6-syngeneic cell line isolated from prostate tumors of *Pten*$^{pc-/-}$*Smad4*$^{pc-/-}$*Trp53*$^{c-/-}$ mice, was generated in 2013. All cell lines tested for *Mycoplasma* were negative within 6 months of performing the experiments. Cell line authentication was not performed.

CyTOF and Flow Cytometry

Prostate tumor single cells were isolated using the Mouse Tumor Dissociation Kit (Miltenyi Biotec). Single cells were isolated from spleen, lymph node, and peripheral blood using standard protocol. All isolated cells were depleted of erythrocytes by hypotonic lysis. For CyTOF analysis, cells were blocked for FcγR using CD16/CD32 antibody (clone 2.4G2, BD Biosciences) and incubated with CyTOF antibody (DVS Sciences, used at 0.5 test/1 million cells) for 30 minutes at room temperature. Cells were washed once and incubated with MAXPARNucleic Acid Intercalator-^{103}Rh (DVS Sciences) for 20 minutes for viability staining. Cells were fixed with 1.6% formaldehyde for 1 hour and incubated with MAXPARNucleic Acid Intercalator-Ir (DVS Sciences) at 4°C overnight to stain the nuclei. The samples were analyzed with CyTOF instrument (DVS Sciences) in the Flow Cytometry and Cellular Imaging Core Facility at the MD Anderson Cancer Center. Flow cytometry was performed using standard protocol on LSRFortessa analyzer (Becton Dickinson) and analyzed with FlowJo software (Tree Star).

T-cell Suppression and MDSC Migration Assay

T-cell suppression assay was performed as described (9) using FACS-sorted MDSCs and CFSE (Invitrogen)-labeled MACS-sorted (Miltenyi Biotec) $CD8^+$ or $CD4^+$ T cells in anti-CD3– and anti-CD28–coated 96-well plates at an MDSC/T-cell ratio of 0:1, 1:1, 1:2, 1:4, with 3.0×10^5 to 5.0×10^5 MDSCs used in each ratio. Cells were analyzed after 72 hours by flow cytometry, and the suppression of T cells is calculated as described (41). The percentage of $CFSE^+$ cells divided in the presence of MDSCs was compared with the percentage of $CFSE^+$ divided cells in the absence of any added MDSCs. For the MDSC migration assay, an equal number of FACS-sorted MDSCs, untreated or pretreated with neutralizing antibody or inhibitor, were placed on the upper chamber of a transwell system (BD Falcon), and conditioned media from PTEN/SMAD4-deficient cells under various conditions were added to the bottom chamber. Cells were allowed to migrate to the bottom well for 6 hours at 37°C with 5% CO_2. Migrated cells were then analyzed by flow cytometry using BD Fortessa X20. Migrated FITC-positive cells were gated to count the absolute number of cells migrated through the transwell.

MSDC Depletion In Vivo with Gr1 Antibody, Peptibody, and CXCR2 Inhibitor SB225002

Anti-Gr1 (clone RB6-8C5) and isotype control (clone LTF2) were purchased from BioXcell and dosed at 200 μg/mouse (i.p.) every other day. Endotoxin-free plasmids (15 μg) for irrelevant control peptibody (Irr-pep) and MDSC-specific Pep-H6 peptibody were injected into mice through tail vein using the established protocol (21) in TransIT-EE Delivery Solution (Mirus Bio LLC) every 4 days. SB225002 (Cayman Chemical) in DMSO was diluted in vehicle (0.9% NaCl, 0.3% Tween 80) for *in vivo* administration every other day (5 mg/kg).

Inducible Yap1 Knockdown

Inducible *Yap1* knockdown was constructed by cloning the two *Yap1* shRNAs used previously (26) from the pLKO.1 into a doxycycline-inducible plasmid. Lentivirus was packaged in 293T and was used to infect PPS, a C57BL/6-syngeneic cell line isolated from prostate tumor of *Pten*$^{pc-/-}$*Smad4*$^{pc-/-}$*Trp53*$^{c-/-}$mice. Stable sublines were selected with puromycin (2 μg/mL) and injected subcutaneously to the flank of 5-week-old male C57BL/6 mice (Jackson Laboratory). Two weeks after injection, mice were fed with doxycycline water (2 g/L), a method used to execute doxycycline-inducible expression *in vivo* (42). Tumors were measured and extracted 6 days later to analyze for MDSC percentage in infiltrating immune cells.

Published OnlineFirst December 23, 2015; DOI: 10.1158/2159-8290.CD-15-0224

Computational Analysis of Mouse Microarray Data and Human Prostate TCGA Data

RNA was isolated from FACS-sorted GFP$^+$ and Tomato$^+$ cells using *Pten*$^{pc-/-}$*Smad4*$^{pc-/-}$*mTmG*$^+$ prostate tumors, followed by microarray analysis at the MD Anderson Microarray Core facility using the Mouse Genome 430 2.0 Array (Affymetrix) to generate a *Pten*$^{pc-/-}$*Smad4*$^{pc-/-}$ tumor/stroma dataset GSE71319. Dataset GSE25140 was downloaded from the NCBI Gene Expression Omnibus (GEO) database. Differentially expressed genes between two conditions (GFP$^+$ vs. Tomato$^+$ or PTEN/SMAD4 vs. PTEN) were subjected to IPA, GSEA, and oPOSSUM analysis. For analysis of human prostate data, we first generated a list of 39 human MDSC signature genes by literature mining (Supplementary Table S7). The gene expression data of 498 TCGA prostate samples were downloaded from the Broad GDAC Firehose (http://gdac.broadinstitute.org), which is the RSEM expression estimates normalized to set the upper quartile count at 1,000 for gene level and then with $\log_2$ transformation. The 498 TCGA prostate samples were clustered using the 39 MDSC genes into MDSC-high, MDSC-low, and MDSC-medium (distance between pairs of samples was measured by Manhattan distance, and clustering was then performed using complete-linkage hierarchical clustering). Sixty-nine samples from Wallace and colleagues (32) were clustered into MDSC-high and MDSC-low. Differentially expressed genes between MDSC-high and MDSC-low were analyzed by GSEA. The expression of *CXCL6* in MDSC-high samples is compared with MDSC-low samples using the Wilcoxon test.

Immunohistochemistry and Western Blot Analysis

Tissues were fixed in 10% formalin overnight and embedded in paraffin. IHC was performed as described earlier (11). For Western blot analysis, cells were lysed on ice using RIPA buffer (Boston BioProducts) supplemented with protease and phosphatase inhibitors (Roche). YAP1 antibody was obtained from Novus Bio and Cell Signaling Technology. CXCL5 antibodies were obtained from Bioss and R&D Biosystems. CXCR2 antibody was obtained from Bioss and R&D Biosystems. CD45 and Ly6G antibodies were obtained from Biolegend. Prostate tissue microarray was obtained from Folio Bioscience.

Chromatin Immunoprecipitation

ChIP was performed as described (26) using YAP1 antibody from Novus. Briefly, 5 μg of rabbit IgG (Santa Cruz) or YAP1 antibody was incubated with Protein A Dynabead magnetic beads (Invitrogen) for 4 hours, followed by extensive wash to remove unbound antibody. Antibody beads were then added to the chromatin and incubated overnight. The following primers were used for qPCR analysis: CXCL5_S: 5′-CTCCAGTTTCCTGCCTGAAG-3′ and CXCL5_as: 5′-GTGTGGAG ATTGGGGCTCTA-3′.

Quantitative RT-PCR

RNA was isolated by the RNeasy Kit (Qiagen) and reverse transcribed using the Superscript III cDNA Synthesis Kit (Life Technology). Quantitative PCR was performed using the SYBR-GreenER Kit (Life Technology). The following primers were used: CXCL5_Fwd: GCATTTCTGTTGCTGTTCACGCTG, CXCL5_Rev: CCTCCTTCT GGTTTTTCAGTTTAGC; β-actin_Fwd: GAAATCGTGCGTGACATC AAAG, β-actin_Rev: TGTAGTTTCATGGATGCCACAG; YAP1_Fwd: TGAGATCCCTGATGATGTACCAC,YAP1_Rev:TGTTGTTGTCTGA TCGTTGTGAT.

Statistical Analysis

Data are presented as mean ± SD unless indicated otherwise. The Student *t* test assuming two-tailed distributions was used to calculate statistical significance between groups. Animal survival benefit was determined by the Kaplan–Meier analysis. $P < 0.05$ was considered statistically significant.

Accession Numbers

The expression array data used in this article were in GEO with accession numbers GSE25140 (11) and GSE71319.

Disclosure of Potential Conflicts of Interest

A. Kapoor is a research investigator at Novartis. C.J. Logothetis has received commercial research grants from Astellas, BMS, J&J, Excelixis, Pfizer, Novartis, Bayer, AstraZeneca, and Helsinn HC. No potential conflicts of interest were disclosed by the other authors.

Authors' Contributions

Conception and design: G. Wang, X. Lu, Z. Ding, C.J. Logothetis, Y.A. Wang, R.A. DePinho
Development of methodology: G. Wang, X. Lu, P. Dey, P. Deng, V. Ramamoorthy, Q. Chang
Acquisition of data (provided animals, acquired and managed patients, provided facilities, etc.): G. Wang, X. Lu, P. Dey, P. Deng, Z. Fang, S. Hua, E.M. Li-Ning-Tapia, Z. Guo, X. Shang, S. Khadka, E.-J. Jin, X. Pan, L. Li, Q. Chang, P. Troncoso, M.J. McArthur
Analysis and interpretation of data (e.g., statistical analysis, biostatistics, computational analysis): G. Wang, X. Lu, P. Dey, C.C. Wu, J. Zhang, C.-J. Wu, N.B. Patel, Y. Shi, Q. Chang, C.J. Logothetis, M.J. McArthur, Y.A. Wang
Writing, review, and/or revision of the manuscript: G. Wang, X. Lu, P. Dey, C.C. Wu, C.-J. Wu, C.J. Logothetis, M.J. McArthur, Y.A. Wang, R.A. DePinho
Administrative, technical, or material support (i.e., reporting or organizing data, constructing databases): P. Dey, P. Deng, C.C. Wu, S. Jiang, R. Konaparthi, E.M. Li-Ning-Tapia, A. Kapoor, N.B. Patel, Z. Guo, T. Heffernan, D. Zhao, X. Shang, P. Hou, B. Hu, W. Yao, Y. Shi, L. Chin
Study supervision: Y.A. Wang, R.A. DePinho
Other (mouse work): K. Zhao
Other (assessed immunohistochemical stains): E.M. Li-Ning-Tapia
Other (supported molecular biology needs, i.e., cloning): T.N. Tieu

Acknowledgments

The authors thank Drs. Larry W Kwak and Hong Qin for the peptibody plasmids; Drs. Willem Overwijk and Yared Hailemichael for advice in hydrodynamic injection; Samirkumar Amin and members of the DePinho laboratory for helpful suggestions and technical support; and the Flow Cytometry and Cellular Imaging Core Facility (Jared Burks, Duncan Mak, and Karen Dwyer) and the Sequencing & Non-coding RNA Core Services (Chang-Gong Liu) at The University of Texas MD Anderson Cancer Center (Cancer Center Support Grant CA16672).

Grant Support

The project was supported by U01CA141508 (to L. Chin and R.A. DePinho), Prostate Cancer Research Program (PCRP) W81XWH-13-1-0202 (to G. Wang) and W81XWH-14-1-0429 (to P. Dey); the Idea Development Award–New Investigator Option (W81XWH-14-1-0576; to X. Lu) from the Department of Defense; and the Clayton & Modesta Williams Cancer Research Fund. Additional support was provided by the Jane Coffin Childs Memorial Fund Postdoctoral Fellowship to X. Lu. E.-J. Jin is supported by Korean Governments (MISP) grant number 2011-0030130.

Received February 23, 2015; revised October 5, 2015; accepted October 16, 2015; published OnlineFirst December 23, 2015.

Published OnlineFirst December 23, 2015; DOI: 10.1158/2159-8290.CD-15-0224

REFERENCES

1. Karlou M, Tzelepi V, Efstathiou E. Therapeutic targeting of the prostate cancer microenvironment. Nat Rev Urol 2010;7:494–509.
2. Junttila MR, de Sauvage FJ. Influence of tumour micro-environment heterogeneity on therapeutic response. Nature 2013;501:346–54.
3. Hanahan D, Coussens L. Accessories to the crime: functions of cells recruited to the tumor microenvironment. Cancer Cell 2012;21: 309–22.
4. Hanahan D, Weinberg Robert A. Hallmarks of cancer: the next generation. Cell 2011;144:646–74.
5. Talmadge JE, Gabrilovich DI. History of myeloid-derived suppressor cells. Nat Rev Cancer 2013;13:739–52.
6. Vuk-Pavlović S, Bulur PA, Lin Y, Qin R, Szumlanski CL, Zhao X, et al. Immunosuppressive CD14+HLA-DRlow/− monocytes in prostate cancer. Prostate 2010;70:443–55.
7. Idorn M, Kollgaard T, Kongsted P, Sengelov L, Thor Straten P. Correlation between frequencies of blood monocytic myeloid-derived suppressor cells, regulatory T cells and negative prognostic markers in patients with castration-resistant metastatic prostate cancer. Cancer Immunol Immunother 2014;63:1177–87.
8. Brusa D, Simone M, Gontero P, Spadi R, Racca P, Micari J, et al. Circulating immunosuppressive cells of prostate cancer patients before and after radical prostatectomy: profile comparison. Int J Urol 2013;20:971–8.
9. Garcia AJ, Ruscetti M, Arenzana TL, Tran LM, Bianci-Frias D, Sybert E, et al. Pten null prostate epithelium promotes localized myeloid-derived suppressor cell expansion and immune suppression during tumor initiation and progression. Mol Cell Biol 2014;34:2017–28.
10. Di Mitri D, Toso A, Chen JJ, Sarti M, Pinton S, Jost TR, et al. Tumour-infiltrating Gr-1+ myeloid cells antagonize senescence in cancer. Nature 2014;515:134–7.
11. Ding Z, Wu CJ, Chu GC, Xiao Y, Ho D, Zhang J, et al. SMAD4-dependent barrier constrains prostate cancer growth and metastatic progression. Nature 2011;470:269–73.
12. Bjornson ZB, Nolan GP, Fantl WJ. Single-cell mass cytometry for analysis of immune system functional states. Curr Opin Immunol 2013;25:484–94.
13. Youn JI, Nagaraj S, Collazo M, Gabrilovich DI. Subsets of myeloid-derived suppressor cells in tumor-bearing mice. J Immunol 2008;181:5791–802.
14. Kusmartsev S, Nefedova Y, Yoder D, Gabrilovich DI. Antigen-specific inhibition of CD8+ T cell response by immature myeloid cells in cancer is mediated by reactive oxygen species. J Immunol 2004;172:989–99.
15. Szuster-Ciesielska A, Hryciuk-Umer E, Stepulak A, Kupisz K, Kandefer-Szerszen M. Reactive oxygen species production by blood neutrophils of patients with laryngeal carcinoma and antioxidative enzyme activity in their blood. Acta Oncol 2004;43:252–8.
16. Schmielau J, Finn OJ. Activated granulocytes and granulocyte-derived hydrogen peroxide are the underlying mechanism of suppression of T-cell function in advanced cancer patients. Cancer Res 2001;61:4756–60.
17. Pekarek LA, Starr BA, Toledano AY, Schreiber H. Inhibition of tumor growth by elimination of granulocytes. J Exp Med 1995;181:435–40.
18. Wang G, Lunardi A, Zhang J, Chen Z, Ala U, Webster KA, et al. Zbtb7a suppresses prostate cancer through repression of a Sox9-dependent pathway for cellular senescence bypass and tumor invasion. Nat Genet 2013;45:739–46.
19. Lunardi A, Ala U, Epping MT, Salmena L, Clohessy JG, Webster KA, et al. A co-clinical approach identifies mechanisms and potential therapies for androgen deprivation resistance in prostate cancer. Nat Genet 2013;45:747–55.
20. Qin H, Lerman B, Sakamaki I, Wei G, Cha SC, Rao SS, et al. Generation of a new therapeutic peptide that depletes myeloid-derived suppressor cells in tumor-bearing mice. Nat Med 2014;20:676–81.
21. Liu F, Song Y, Liu D. Hydrodynamics-based transfection in animals by systemic administration of plasmid DNA. Gene Ther 1999;6: 1258–66.
22. Muzumdar MD, Tasic B, Miyamichi K, Li L, Luo L. A global double-fluorescent Cre reporter mouse. Genesis 2007;45:593–605.
23. Yang L, Huang J, Ren X, Gorska AE, Chytil A, Aakre M, et al. Abrogation of TGF beta signaling in mammary carcinomas recruits Gr-1+CD11b+ myeloid cells that promote metastasis. Cancer Cell 2008;13:23–35.
24. Bierie B, Stover DG, Abel TW, Chytil A, Gorska AE, Aakre M, et al. Transforming growth factor-beta regulates mammary carcinoma cell survival and interaction with the adjacent microenvironment. Cancer Res 2008;68:1809–19.
25. Johnson R, Halder G. The two faces of Hippo: targeting the Hippo pathway for regenerative medicine and cancer treatment. Nat Rev Drug Discov 2014;13:63–79.
26. Kapoor A, Yao W, Ying H, Hua S, Liewen A, Wang Q, et al. Yap1 activation enables bypass of oncogenic Kras addiction in pancreatic cancer. Cell 2014;158:185–97.
27. Shao DD, Xue W, Krall EB, Bhutkar A, Piccioni F, Wang X, et al. KRAS and YAP1 converge to regulate EMT and tumor survival. Cell 2014;158:171–84.
28. Zhao B, Li L, Wang L, Wang CY, Yu J, Guan KL. Cell detachment activates the Hippo pathway via cytoskeleton reorganization to induce anoikis. Genes Dev 2012;26:54–68.
29. Nguyen LT, Tretiakova MS, Silvis MR, Lucas J, Klezovitch O, Coleman I, et al. ERG activates the YAP1 transcriptional program and induces the development of age-related prostate tumors. Cancer Cell 2015;27:797–808.
30. Kwon AT, Arenillas DJ, Worsley Hunt R, Wasserman WW. oPOSSUM-3: advanced analysis of regulatory motif over-representation across genes or ChIP-Seq datasets. G3 2012;2:987–1002.
31. Ding Z, Wu C-J, Jaskelioff M, Ivanova E, Kost-Alimova M, Protopopov A, et al. Telomerase reactivation following telomere dysfunction yields murine prostate tumors with bone metastases. Cell 2012;148:896–907.
32. Wallace TA, Prueitt RL, Yi M, Howe TM, Gillespie JW, Yfantis HG, et al. Tumor immunobiological differences in prostate cancer between African-American and European-American men. Cancer Res 2008;68:927–36.
33. Chen Z, Trotman LC, Shaffer D, Lin HK, Dotan ZA, Niki M, et al. Crucial role of p53-dependent cellular senescence in suppression of Pten-deficient tumorigenesis. Nature 2005;436:725–30.
34. Liu Q, Russell MR, Shahriari K, Jernigan DL, Lioni MI, Garcia FU, et al. Interleukin-1beta promotes skeletal colonization and progression of metastatic prostate cancer cells with neuroendocrine features. Cancer Res 2013;73:3297–305.
35. Toh B, Wang X, Keeble J, Sim WJ, Khoo K, Wong WC, et al. Mesenchymal transition and dissemination of cancer cells is driven by myeloid-derived suppressor cells infiltrating the primary tumor. PLoS Biol 2011;9:e1001162.
36. Stromnes IM, Brockenbrough JS, Izeradjene K, Carlson MA, Cuevas C, Simmons RM, et al. Targeted depletion of an MDSC subset unmasks pancreatic ductal adenocarcinoma to adaptive immunity. Gut 2014;63:1769–81.
37. Gabrilovich DI, Ostrand-Rosenberg S, Bronte V. Coordinated regulation of myeloid cells by tumours. Nat Rev Immunol 2012;12:253–68.
38. Osanto S, van Poppel H, Burggraaf J. Tasquinimod: a novel drug in advanced prostate cancer. Future Oncol 2013;9:1271–81.
39. Filipazzi P, Huber V, Rivoltini L. Phenotype, function and clinical implications of myeloid-derived suppressor cells in cancer patients. Cancer Immunol Immunother 2012;61:255–63.
40. Solito S, Marigo I, Pinton L, Damuzzo V, Mandruzzato S, Bronte V. Myeloid-derived suppressor cell heterogeneity in human cancers. Ann N Y Acad Sci 2014;1319:47–65.
41. Battaglia M, Stabilini A, Roncarolo MG. Rapamycin selectively expands CD4+CD25+FoxP3+ regulatory T cells. Blood 2005;105:4743–8.
42. Ying H, Kimmelman AC, Lyssiotis CA, Hua S, Chu GC, Fletcher-Sananikone E, et al. Oncogenic Kras maintains pancreatic tumors through regulation of anabolic glucose metabolism. Cell 2012;149: 656–70.